Regulation of NLRP3 Inflammasome Activation by TRAF1 in Murine Models of Inflammasome-Driven Disease

Jonathan Raspanti

A THESIS SUBMITTED TO
THE FACULTY OF GRADUATE STUDIES
IN PARTIAL FULFILLMENT OF THE REQUIREMENTS
FOR THE DEGREE OF
MASTER OF SCIENCE

GRADUATE PROGRAM IN KINESIOLOGY AND HEALTH SCIENCE
YORK UNIVERSITY
TORONTO, ONTARIO

August 2021

Abstract

The NLRP3 inflammasome is a multimeric protein complex that plays a crucial role in the activation and release of IL-1β. Unpublished in-vitro research from our lab highlights the signalling adaptor protein tumor necrosis factor receptor (TNFR) associated factor 1 (TRAF1) is an important regulator of the NLRP3 inflammasome. Understanding this regulation in-vivo is important because dysregulation of TRAF1 and the NLRP3 inflammasome is implicated in the pathogenesis of autoinflammatory diseases. To this end, two NLRP3 inflammasome-dependent in-vivo models were employed in wild-type (WT) and TRAF1 deficient ($TRAF1^{-/-}$) mice. In the MSU-induced peritonitis model, $TRAF1^{-/-}$ mice showed increased recruitment of inflammatory leukocytes, while in the crystal-induced arthritis model, $TRAF1^{-/-}$ exhibited a marked increase in knee joint inflammation and expression of pro-inflammatory genes. Altogether, we demonstrate that TRAF1 plays an important role in controlling inflammasome activation and inflammasome-driven diseases, which provides insights that could lead to improved outcomes of NLRP3 inflammasome-related diseases.

Acknowledgement

The phrase “it takes a village” could not be more true in the preparation of this thesis. Thank you to everyone, named below or not, for your unwavering support.

Firstly, I would like to thank Dr Ali Abdul-Sater for the invaluable teachings, mentorship, and support through my multiple roles in his lab. Thanks to your guidance and commitment to me as my supervisor, I have been able to grow and achieve so much, and I am very grateful. Thank you for the opportunity to learn about and pursue research.

Thank you Safoura, Fatemah, Sunpreet, Bipan, Mayoorey, Amandeep, Yitian, Ali A. and Ali M. for teaching and/or assisting me with the experiments in this paper. I also cannot thank you all enough for all of your support and friendship. Also, thank you to my thesis committee, Dr Christopher Perry, and Dr Peter Backx for all of your commitment and contributions to helping me complete my thesis.

I am also very appreciative of all the administrative support from the Faculty of Graduate Studies and School of Kinesiology and Health Science for helping me make the circumstances of this thesis submission a reality.

Thank you, mom, dad, and Justin, for always being there to care for, cheer me on and encouraging me to be the person I am today.

Finally, thank you Sabrina for being in my corner since day one and always being the first person to keep me focused on making my goals reality.

Table of Contents

List of Figures

List of Tables

List of Abbreviations

AA	Amino Acid
AIM2	Absent-in melanoma 2
ALRs	Absent-in-melanoma 2 (AIM2)-like receptors
ASC	Apoptosis-associated speck-like protein containing a CARD
ATP	Adenosine triphosphate
BIRs	Baculovirus inhibitor repeat motif
CAPS	Cryopyrin-associated periodic syndromes
CARD	Caspase recruitment domain
cIAP	Cellular inhibitor of apoptosis protein
CLRs	C-type lectin receptors
CPPD	Calcium pyrophosphate dihydrate
CRISPR/Cas9	Clustered regularly interspaced short palindromic repeats
DAMPs	Calcium pyrophosphate dihydrate
DNA	Deoxyribonucleic acid
GSDMD	Gasdermin D
HDR	Homology-directed repair
HOIL-1	Heme-oxidized IRP2 ubiquitin ligase-1
HOIP	HOIL-1–interacting protein
IKK	IκB kinase
ILs	Interleukins
IL-1	Interleukin-1
IL-1β	Interleukin-1β
IL-6	Interleukin-6
IL-12	Interleukin-12
IL-18	Interleukin-18
IL-1R	Interleukin-1 receptor
KO	Knockout
LPS	Lipopolysaccharide
LRR	Leucine-rich repeats
LUBAC	Linear ubiquitin chain assembly complex
MSU	Monosodium urate
mtDNA	Mitochondrial DNA
mtROS	Mitochondrial ROS
MyD88	Myeloid differentiation primary response protein 88
NACHT	NLR nucleotide-binding domain
NEMO	NF-κb Essential Modulator
NF-κB	Nuclear factor-κb
NLR	Nucleotide-binding oligomerization domain (NOD)-like receptors
NLRP	NOD-like receptor protein
NLRP3	NLR and pyrin domain-containing protein 3
NOD	Nucleotide-binding oligomerization domain

P	Phosphorylation
PAMPs	Pathogen-associated molecular patterns
PGNs	Peptidoglycans
PI3K	Phosphatidyl-inositol 3-kinase
PRRs	Pattern recognition receptors
PYD	Pyrin domain
pyk2	Protein-tyrosine kinase 2β
RA	Rheumatoid arthritis
RIG-I	Retinoic acid-inducible gene I
RLRs	Retinoic acid-inducible gene I (RIG-I)-like receptors
RNA	Ribonucleic acid
ROS	Reactive oxygen species
S	Sumolyation
SHARPIN	Shank-associated RH domain interactor
SN	S-nitrosylation
SNPs	Single nucleotide polymorphisms
Src	Proto-oncogene tyrosine-protein kinase Src
TIR	Toll/IL-1 receptor
TLR	Toll-like receptors
TNF	Tumor necrosis factor
TNFR	Tumor necrosis factor receptor
TRAF	Tumor necrosis factor receptor (TNFR)-associated factor
TRAF1	Tumor necrosis factor receptor (TNFR)-associated factor 1
Ub	Ubiquitination
WT	Wild type

Chapter One: Literature Overview

1.1 Pathogen and Danger Associated Molecular Patterns (PAMPs and DAMPS)

Inflammasomes are macro-molecular protein complexes that are formed within the cytosol of innate immune cells[1,2]. Inflammasomes play an important role in detecting and responding to various signals indicative of pathogens and tissue damage[3]. The first step of inflammasome activation is the assembly of the inflammasome complex, which requires the recognition of small molecular motifs called pathogen-associated molecular patterns (PAMPs)[4]. PAMPs include bacterial structural components, such as lipopolysaccharide (LPS) and peptidoglycans (PGNs), or viral RNA[5]. Following this, danger-associated molecular patterns (DAMPS), which are endogenous molecular patters released following damage incurred to cells and tissues lead to the activation of inflammasomes[6]. DAMPs can include signals induced by molecules such as DNA, RNA or uric acid, which are not normally present in certain cellular locations[5]. Once activated, inflammasomes facilitate the activation of the proteolytic enzyme caspase-1, which cleaves the inactive pro-form of interleukins (ILs) IL-1β and IL-18 into their biologically active forms. Secretion of active IL-1β and IL-18 is an independent process that is also mediated by activated caspase-1. To do so, caspase-1 cleaves and activates Gasdermin D, which in turn releases its N-terminal fragment to mediate IL-1β secretion as well as programmed cell death known as pyroptosis[1,6,7].

1.2 Pattern Recognition Receptors (PRRs)

Pattern recognition receptors (PRRs) recognize common molecular structures shared by a wide-range of dangerous components associated with toxins, cellular damage and pathogenetic microorganisms[8]. PRRs are germline encoded sensors that are expressed on the surface of immune cells, and stimulate responses that are characteristic of the innate immune response[6,9].

These sensors activate signalling cascades that promote the proliferation of molecules like chemokines, cytokines, antibacterial peptides and interferons[9]. PRRs can be subdivided into families of membrane bound toll-like receptors (TLRs), cytoplasmic nucleotide-binding oligomerization domain (NOD)-like receptors (NLRs), retinoic acid-inducible gene I (RIG-I)-like receptors (RLRs), absent in melanoma 2 (AIM2)-like receptors (ALRs) and C-type lectin receptors (CLRs)[6,9–11].

Of particular interest are TLRs and NLRs, as they both play roles in the formation and activation of the NLRP3 inflammasome[3]. So far, TLRs include a family of at least 10 members in humans and 13 in mice[12]. They share high similarity to the interleukin 1 receptor (IL-1R) family in the cytoplasmic portion of the receptors, however, unlike IL-1 receptors, TLRs express characteristic leucine-rich repeats (LRRs) in their extracellular domain[13,14]. TLRs are found on the plasma membrane or on various components inside of immune cells like monocytes, macrophages, dendritic cells, B lymphocytes, T lymphocytes and mast cells, in addition to non-immune cells like epithelial cells, endothelial cells and fibroblasts[6,15,16]. TLRs recognize a wide-range of specific microbial components derived from pathogens, like lipids, lipoproteins, and proteins[16]. For example, TLR4 plays a critical role in recognizing ligands like LPS present on gram-negative bacteria[13,17].

TLRs sense a variety of ligands either alone or in combination with other TLRs by triggering ligand-induced dimerization of the receptors. Then, the Toll/IL-1 receptor (TIR) domain of TLRs bind to TIR domain-containing adaptor proteins like myeloid differentiation primary response protein 88 (MyD88)[12,18]. The signalling cascade following activation of TLR leads to activation of nuclear factor-κB (NF- κB) present in the cytoplasm[19]. Once active, NF-κB translocates to the nucleus where it can bind the promoters of genes containing specific NF-kB-

binding sequence, including that of NOD, LRR (NLR) and pyrin domain-containing protein 3 (NLRP3), pro-IL-1β, pro-IL-18, apoptosis-associated speck-like protein containing a caspase recruitment domain (CARD) (ASC), caspase-1, and other pro-inflammatory cytokines like IL-6, IL-12 and TNFα [5,14,19,20]. Aside from pro-IL-1β and pro-IL-18, the other pro-inflammatory cytokines are biologically active once transcribed and are subsequently secreted from the cell.

NLRs are intracellular cytoplasmic sensors primarily expressed in macrophages and other antigen-presenting cells, but are also present in lymphocytes and other non-immune cells[12]. NLRs recognize signals of endogenous cellular injury and stress (DAMPs) as well as conserved microbial and viral components (PAMPs)[21]. Currently, there are 22 known members of the NLR family in humans and at least 33 NLR genes in mice[22,23]. NLRs share a similar C-terminal LRR domain that binds ligands like DAMPs and PAMPs, a central nucleotide-binding domain (NACHT) which is critical for self-oligomerization, and a variable N-terminal domain[12,21]. NLRs are subdivided on the based on this N-terminal domain, and include (i) NLRA, A for acidic transactivating domain, (ii) NLRB, B for baculovirus inhibitor repeat motif (BIRs), (iii) NLRC, where C stands for CARD, and (iv) NLRP, where P stands for a pyrin domain (PYD)[12]. NLRs can be activated by a wide-range of stimuli including extracellular ATP, activators that form crystalline structures like MSU or asbestos, and mechanisms that trigger the generation of reactive oxygen species (ROS) like mitochondrial damage[24].

1.3 Canonical Inflammasomes

Inflammasomes are multimeric protein complexes that form in the cytosol after sensing PAMPs or DAMPs. In general, canonical inflammasomes serve as large protein complexes that recruit the inactive zymogen pro-caspase-1[3,4,25,26]. To accomplish this, the first component of the

inflammasome, which is a receptor, must detect an inflammatory ligand or danger event. To date, at least five sensor proteins have been confirmed to assemble inflammasomes; NLRP1, NLRP3, NLRC4, AIM2 and pyrin[3,20,26]. Following activation of the receptor, these proteins undergo oligomerization into active protein complexes that form a pro-caspase-1 activating platform[3,20,27]. Since most sensors that form inflammasomes lack a CARD, they cannot directly recruit caspase-1 and thus require the adaptor protein, ASC to do so[20,28,29]. The result is the proximity-induced autocleavage[30] required to form activated caspase-1, a proteolytic enzyme that is responsible for processing pro-IL-1β and pro-IL-18 into their biologically active forms, IL-1β and IL-18[24,31,32]. IL-1β is produced as a 269-amino acid (AA) precursor protein and when processed by caspase-1 apart of the activated in inflammasomes, to the C-terminal 153 AA as mature IL-1β[33]. IL-1β is a potent cytokine, so its secretion is tightly regulated by the assembly of the inflammasome complex before it can be released. When IL-1β secretion is dysregulated, studies have shown it to be implicated in the pathogenesis of many diseases, in particular rheumatoid arthritis (RA)[34–36]. Active caspase-1 also cleaves Gasdermin D, which forms pores in the plasma membrane and triggers a lytic, pro-inflammatory form of cell death, termed pyroptosis[4,20].

1.4 NLRP3 Inflammasome

The most widely studied and best characterized inflammasome complex is NLRP3. Most inflammasome receptors, including NLRP3, lack a CARD motif and cannot interact directly with caspase-1. In order to interact with caspase-1, NLRP3 inflammasomes require an amino-terminal PYD of the bipartite adaptor ASC to interact with the upstream NLRP3 receptor and subsequently recruit caspase-1 through its carboxy-terminal CARD[27,31]. Following this, rapid oligomerization of ASC occurs via PYD-PYD interactions and creates multiple potential activation sites for caspase-1[29]. At the activation sites, pro-caspase-1 interacts with ASC

‘specks’ via CARD-CARD interactions and proteolytic cleavage occurs to facilitate the active caspase-1[29]. As mentioned above, active caspase-1 proteolytically processes pro-IL-1β and pro-IL-18 into their mature forms and facilitates the active form of Gasdermin D, leading to pyroptosis[3,26,28].

IL-1β is an important proinflammatory mediator that is generated at sites of injury, infection or immunological dysregulation to coordinate a wide-range of responses including cellular recruitment to a site of infection or injury and the regulation of sleep, appetite, and body temperature[24,33,37]. Since the downstream effects of IL-1β are so powerful and robust, full activation of the NRLP3 inflammasome requires two signals that are indicative of cellular damage or stress. The first signal is that of PAMPs, which can include bacterial toxins like LPS that act on TLRs to promote NF-κB-dependent transcription of NLRP3 and pro-IL-1β[4,20,38]. This first signal and downstream transcription are referred to as priming or signal 1. Other stimuli known to activate NF-κB, such as tumor necrosis factor (TNF), Pam3CSK, and IL-1 have also been shown to fulfil the requirements of the priming step before the initiation of signal 2[39].

The second signal required to fully activate the NLRP3 inflammasome can be achieved by several PAMPs or DAMPs. NLRP3-activating PAMPs include; bacteria-derived RNA or DNA, pore-forming toxins like nigericin, lethal toxins, flagellin/rod proteins, muramyl dipeptide (MDP), M2 protein, virus-derived RNA or DNA, fungus-derived β-glucans, hypha mannan, zymosan, and protozoon-derived hemozoin[26,33,40]. DAMPs that have been shown to activate NLRP3 include; self-derived glucose, β-amyloid, hyaluronan, extracellular ATP, cholesterol crystals, monosodium urate (MSU) crystals, calcium pyrophosphate dihydrate (CPPD) crystals, environment-derived alum, asbestos, silica, alloy particles, UV radiation, and skin irritants[26,33,40]; Although the specific signalling pathways that lead to NLRP3 activation from the

aforementioned signals is not fully understood, it is generally accepted that these stimuli do not interact with the NLRP3 itself, rather they trigger pathways that lead to; production of ROS, lysosomal damage, mitochondrial damage, translocation of NLRP3 to mitochondria, potassium efflux, calcium mobilization, and others[4,20,25,26]. Upon detection of these processes, NLRP3 becomes active to initiate its oligomerization and interaction with ASC; which then facilitates the recruitment, cleavage and activation of caspase-1[3,20,24].

Although there are many agonists to NLRP3 activation, an all-encompassing model of NLRP3 inflammasome activation is speculative. However, there are several common features that are generally agreed upon, including cytosolic ion concentrations and mitochondrial damage[41]. One such signal is the decrease in cytosolic K^+ observed upon cellular exposure to extracellular ATP, pore-forming toxins (like nigericin), and particulates[42]. K^+ efflux precedes mitochondrial dysfunction and has been shown to correlate with inflammasome activation in various models controlling extracellular K^+ concentrations[20,41,43]. Although incompletely understood, cytosolic K^+ levels might participate, directly or indirectly, in the conformational changes of NLRP3 oligomers in inflammasome activation[41]. Before the discovery of the inflammasome, studies examining ATP and nigericin (which are now known to be NLRP3 stimuli) promote mature IL-1β secretion via cytosolic depletion of K^+[20]. One method of K^+ efflux is through binding of extracellular ATP to P2X7 receptor ATP-gated ion channel, which triggers K^+ efflux and formation of pores in the membrane, mediated by pannexin-1 channel, and thereby activating NLRP3[41,44]. Another study indicated that the K^+ efflux channel TWIK2 in macrophages has a fundamental role in ATP-induced NLRP3 inflammasome activation and therefore plays a role in mediating inflammation[43]. K^+ efflux may also promote Ca^{2+} influx, which activates NLRP3 and promotes the interaction between NLRP3 and ASC[20,41,45]. Ca^{2+} also

binds to proteins S100A8 and S100A9, which often exist as a heterodimer expressed in neutrophils and monocytes. S100A8/A9 is a Ca^{2+} sensor that is released actively during inflammation and exerts a critical role in modulating the inflammatory response by stimulating leukocyte recruitment and inducing cytokine secretion[46].

Studies have also suggested that increases in cytosolic Ca^{2+} overload the mitochondria and induce mitochondrial dysfunction leading to NLRP3 activation[45]. Many DAMPs that could interact with NLRP3 arise following mitochondrial damage, like the production of mitochondrial ROS (mtROS) and release of mitochondrial DNA (mtDNA), among others[20,41]. The role of mtROS and mtDNA as an activator of the NLRP3 inflammasome is contested; most studies examining mitochondrial dysfunction use chemical inhibitors that cause artifacts which may also block the priming signal required for NLRP3 inflammasome activation[20]. One study even showed that mitochondrial dysfunction is not required for NLRP3 activation[42]. Aside from mtROS or mtDNA production, some studies have indicated that, when stimulated, NLRP3 translocates to mitochondria (also potentially the endoplasmic reticulum or Golgi network) to use it as a scaffold for its assembly[20].

A commonly used model to activate and assess NLRP3 inflammasome activation and downstream modulation is through the use of MSU, which is the culprit behind gouty arthritis, the most common inflammatory arthritis in adults[47]. MSU, among other particulates, is phagocytosed by macrophages and mediates the release of IL-1β by promoting the activation of the NLRP3 inflammasome[47,48]. Disruption of lysosomes following phagocytosis of particulates may lead to the release of lysosomal Ca^{2+} into the cytosol and participate in the rise of cytosolic Ca^{2+} levels, activating the NLRP3 inflammasome[41,45]. Concurrently, the active secretion of the Ca^{2+} sensor S100A8/A9, which has been correlated with disease progression of gout, is

upregulated in synovia and sera. S100A8/A9 is secreted by neutrophils and monocyte-derived macrophages that have been recruited to the infection site to accelerate inflammation[49]. MSU plays a crucial role in recruitment of these cells and subsequent secretion of S100A8/A9, which also enhances MSU-induced NLRP3 activation[46].

MSU can also act as a potent stimulator of the NLRP3 inflammasome via the secretion of cathepsins from lysosomes[50–52]. In particular, Phosphatidyl-inositol 3-kinase (PI3K), Protein-tyrosine kinase 2β (Pyk2) and Proto-oncogene tyrosine-protein kinase Src (Src) are activated during the phagocytosis of MSU and subsequently facilitate the secretion of mature cathepsins[52]. Secreted mature cathepsins are involved in the activation of apoptotic pathways and act as a DAMP detected by NLRP3, enabling its activation and inflammasome formation[50]. A study has also shown that Cathepsin B plays a role in facilitating the interactions between NLRP3 and ASC in inflammasome activation[51]. Previous work from our lab has also shown that NLRP3 inflammasome activation is enhanced by MSU without the need of LPS priming beforehand. This means that signal 1, and downstream NF- κB activation is not essential to promoting NLRP3 inflammasome activation. Therefore, standardized protocols have been developed and perfected to use MSU as both an in-vitro and in-vivo activator of the NLRP3 inflammasome for its subsequent analysis[53].

The components of the NLRP3 inflammasome also undergo a variety of post-translational modifications that are essential for appropriate protein regulation[54]. These modifications influence the activity, degradation, localization, structure and interactions with other proteins of the NLRP3 inflammasome[44]. These post-translational modifications including ubiquitination (Ub), phosphorylation (P), sumolyation (S), and s-nitrosylation (SN)[20,44]. Of these, the ubiquitin system plays a crucial role in regulating inflammasome activation[55,56]. More

specifically to NLRP3 inflammasome activation, the linear ubiquitin chain assembly complex (LUBAC), which consists of heme-oxidized IRP2 ubiquitin ligase-1 (HOIL-1), HOIL-1–interacting protein (HOIP) and the Shank-associated RH domain interactor (SHARPIN) is responsible for key post-translational modifications[57].

1.5 NLRP3 Inflammasome and Disease

Dysregulation of NLRP3 inflammasomes via a gain-of-function mutation in and around the NLRP3 NACHT domain has also been associated with cryopyrin-associated periodic syndromes (CAPS), an autoinflammatory disease in which patients experience rashes, prolonged fever and even cognitive defects[31]. Another set of single nucleotide polymorphisms (SNPs) in the NLRP3 promotor region has been associated with Crohn's disease in humans too[31]. A recent review notes that inflammasome dysfunction has been cited in diseases like type-2 diabetes, atherosclerosis, heart and liver diseases, Parkinson's disease, Alzheimer's disease and most relevant to this study, RA[35]

RA is a common autoimmune disorder that affects about 1% of the population worldwide. The disease is characterized by persistent articular inflammation and joint damage driven by the proliferating synovial tissue fibroblasts, T and B lymphocytes, neutrophils and monocytes migrating into the synovium[29]. The irreversible joint destruction and synovial inflammation that RA causes contributes to motor impairment and premature mortality[58]. Human and mouse-based studies show that mRNA and protein expression of inflammasome components are increased in RA patient synovial fluids and circulating macrophages/monocytes, neutrophils, and dendritic cells. These studies propose that NLRP3 activation is involved in both systemic and local inflammation in RA[35,59–61]. Other studies have shown that patients with active RA have increased expression of NLRP3 and NLRP3-mediated IL-1β secretion in whole blood cells[60,62].

These, and many more studies suggest the important role that the NLRP3 inflammasome plays in modulating the pathogenesis of RA[60,63]. Current evidence has not yet demonstrated the exact mechanism by which the NLRP3 inflammasome is in involved in the pathophysiology of RA, however, it has been suggested that NLRP3-induced IL-1β activation contributes to manipulating and maintaining the inflammatory processes in RA and the NLRP3 inflammasome may be a suitable pharmacological target of RA treatment[35,61].

1.6 TRAF1

The tumor necrosis factor receptor (TNFR)-associated factor (TRAF) family of six intracellular proteins that were originally identified as signaling adaptors that bind directly to the cytoplasmic regions of receptors of the TNF-R family[64]. TRAFs are major signal transducers for the TNFR, TLR and NLR signalling pathways. Cellular functions ranging from innate and adaptive responses, tissue homeostasis, and stress responses are mediated by TRAFs through the promotion of numerous cellular processes[64].

Tumor necrosis factor receptor associated factor 1 (TRAF1) is a signaling adaptor that has recently been shown to negatively regulating TLR and NLR signaling, independent of its role in TNFR signalling[57,65]. TRAF1 is a unique member of the TRAF family as it lacks a RING finger domain that is present in TRAF 2-6. TRAF1 expression is restricted to activated lymphocytes, dendritic cells and myeloid cells[64,66]. TRAF1's role in signalling is context-dependent; it can promote NF-κB expression downstream of TNFR in lymphocytes, but also limit NF-κB through inhibiting the linear ubiquitination that is required to induce inflammation downstream of TLRs in monocytes[57,65,67].

1.7 TRAF1 and Inflammasomes

Downstream of TNFR in lymphocytes, TRAF1 promotes NF-κB activation by forming a heterotrimer with TRAF2 that recruits cellular inhibitor of apoptosis protein (cIAP) to the TNFR in lymphocytes[64,65]. This helps promote the priming step, or signal 1 required for inflammasome formation.

However, in monocytes, TRAF1 has been demonstrated to negatively regulate NF-κB activation downstream of activated TLRs[57]. This occurs through interaction with the components of LUBAC. Specifically downstream of TLR activation, multiple signaling processes are activated that lead to activation of IκB kinase (IKK) comprising two catalytic subunits (IKKα, IKKβ) and a regulatory subunit IKKγ (NEMO). Activation of IKK results in phosphorylation of IκBα and its K48-linked poly-ubiquitination followed by degradation in the 26S proteasome[12,68]. This results in translocation of NF-κB from the cytoplasm to the nucleus and binding to promoter elements[19]. LUBAC has been shown to linearly ubiquitinate NEMO and therefore regulate the downstream activation of NF-κB[68,69]. Abdul-Sater et al. have shown that TRAF1's interaction with all three components of LUBAC suppresses its ability to interact with NEMO and ultimately decreases NF-κB activation[57].

Aside from modulating NF-κB activation, the HOIL-1 subunit of LUBAC mediates linear ubiquitination of ASC adaptor proteins that are responsible for the assembly of the ASC/NLRP3 complex and subsequent NLRP3 inflammasome activation[55,70]. **Figure 1** summarizes TRAF1 and NLRP3 inflammasome signalling pathways. Understanding the mechanism in which TRAF1 regulates NLRP3 inflammasome activation via its interaction with LUBAC would provide great insight into the pathogenesis of chronic autoinflammatory and autoimmune diseases like gout and RA[61,71].

1.8 Our Lab's Current Research

Our lab has identified the site of interaction between TRAF1/cIAP2 downstream of TNFR, and TRAF1/LUBAC downstream of TLR using site-directed mutagenesis. A mutant variant of TRAF1, including V203A fails to interact with cIAP2 while maintaining complete interaction with HOIL-1 subunit of LUBAC. Another mutant of TRAF1 (S283A), fails to bind LUBAC without affecting interaction with cIAP2. Using CRISPR/Cas9 homology directed repair, we have been able to successfully create and identify THP-1 human monocytic leukemia cells that express TRAF1 with the V203A mutation. We are in the process of using the same method to introduce the S283A mutation.

We will use the cells with these altered amino acid residues to assess markers of inflammasome assembly, which occurs independently of TLR signalling (signal 1). This way, we can examine the role that TRAF1 plays in NLRP3 inflammasome activation via its interaction with LUBAC.

Through in-vitro studies on THP1 cells, our lab has provided insight into the intracellular mechanism of NLRP3 inflammasome activation in the absence of TRAF1. Using shRNA TRAF1 knockdown cells that exhibit lower TRAF1 expression, there was increased linear ubiquitination and oligomerization of ASC adaptor protein, which resulted in increased recruitment of active caspase-1 and mature IL-1β secretion. We demonstrated that TRAF1 can play an important role in regulating NLRP3 inflammasome activation by limiting caspase-1 activation and IL-1β secretion via its interaction with LUBAC. Our lab has also demonstrated that NF-κB signalling is not essential in promoting NLRP3 activation through use of MSU crystals without the application of priming, or signal 1.

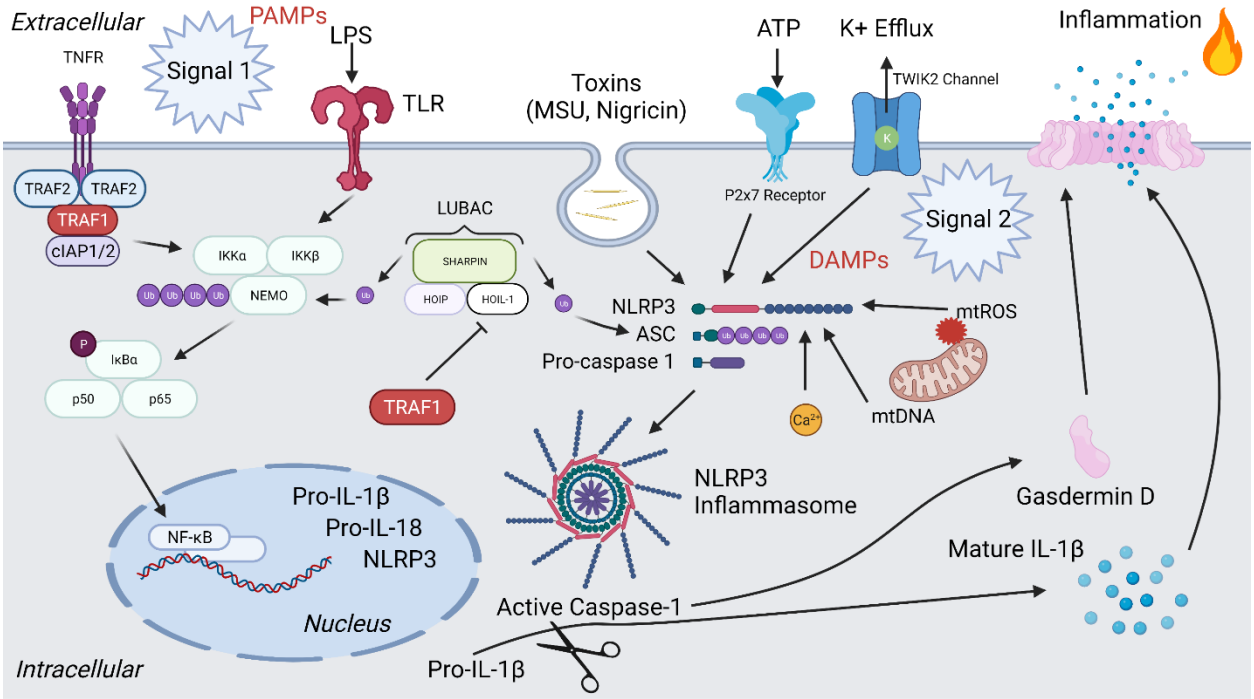

Figure 1. *An overview of TRAF1-mediated regulation of NLRP3 inflammasome activation.*

Chapter Two: Rationale and Objectives

2.1 Rationale

Previous in-vitro studies were important to identify the mechanism through which TRAF1 regulates inflammasome activation by inhibiting caspase-1 recruitment and secretion of mature IL-1β via the NLRP3 inflammasome in the human monocytic cell line, THP-1. However, whether TRAF1 can modulate inflammasome activation in-vivo remains unclear. Moreover, how and if this can affect inflammasome-driven diseases remains unexplored.

In this study, I will first confirm that the previous major findings obtained from the THP-1 cell line will also apply to primary mouse bone-marrow derived macrophages. Then, we will move to the in-vivo models of inflammasome activation and inflammasome-driven disease. If our previous findings hold true in-vivo and in disease models, we can be more confident on the implications of TRAF1 as a potential target for reducing the inflammatory response in autoinflammatory and autoimmune diseases like RA. I will also explore the effect that the TRAF V203A mutation has on NLRP3 inflammasome activation and determine the significance of the specific interaction between TRAF1 and cIAP2 on downstream inflammation. Given that NLRP3 inflammasome components and downstream effector molecules have been shown to be present and elevated in patients with RA, this research could unlock insight into the mechanisms in which the NLRP3 inflammasome contributes to the pathogenesis of RA.

2.2 Objectives

The main objectives of this study are to:

1. Determine whether NLRP3 inflammasome activation is altered in TRAF1 knockout mice.
2. Investigate the role of TRAF1 in NLRP3 inflammasome activation and innate immune cell infiltration using an MSU-induced peritonitis model; an in-vivo murine model of NLRP3 inflammasome-dependent inflammation.
3. Elucidate TRAF1's role in NLRP3 inflammasome activation in crystal-induced arthritis; an in-vivo murine model of NLRP3 inflammasome-dependent inflammatory arthritis.
4. Examine whether the TRAF1 V203A mutation alters NLRP3 inflammasome activation in-vitro.

2.3 Hypothesis

We hypothesize that TRAF1 controls NLRP3 inflammasome activation and subsequent inflammation in-vivo. We expect TRAF1's absence to result in increased peritonitis and inflammatory arthritis in the two examined murine models of NLRP3 inflammasome-dependent disease. We also expect NLRP3 inflammasome activation to be unaffected by the TRAF1 V203A mutation.

Chapter Three: Methods

3.1 Cell Culture

Murine bone marrow derived macrophages and THP-1 human monocytic leukemia cells (Sigma-Aldrich) were cultured in a humidified incubator at 37°C with 20% O_2 and 5% CO_2 in RPMI 1640 (Sigma-Aldrich) supplemented with 10% heat-inactivated fetal bovine serum (Multicell), 2-Mercapthoethanol (2-ME) (Gibco), 1% L-Glutamine-Pyruvate-Penicillin-Streptomycin (GPPS), and non-essential amino acids (Sigma). For THP-1 cells, RMPI media was replenished every 48 hours and the cells were kept at a concentration of 1×10^6 cells/mL in about 10 mL of RPMI media.

3.2 Mice Genotyping

Once C57BL/6 mice pups were weaned from their mothers, small (< 5 mm) clippings of their tail were received from our animal care facility to determine the genotype of each mouse. Genomic DNA was extracted and amplified using the REDExtract-N-Amp Tissue PCR Kit (Sigma-Aldrich). Each mouse tail was emersed in a mixture of 50 μL of extraction solution and 12.5 μL of tissue preparation solution in a 1.5 mL microcentrifuge tube. The tails incubated at room temperature for 10 minutes and then transferred to a 95 ˚C heating block for 3 minutes. Next, 50 μL of neutralization solution was added to each sample and mixed by vortexing.

1 μL of genomic DNA from each sample was combined with 3 μL of DNAsa and RNAse free water (Life Technologies), 5 μL of KAPA2G Fast Genotyping Mix (Sigma-Aldrich), and 0.5 μL of the forward (10 mM) and reverse primer (10 mM) to detect the TRAF knockout (KO) genotype. Primers used are outlined in **Table 1**. Another 1 μL of each genomic DNA sample was combined with the same components above, but with primers detecting the wild-type (WT) genotype. The samples were mixed by pipetting up and down and centrifuged briefly to bring all

contents to the bottom of the 200 µL PCR tube. The samples were then placed in a thermo-cycler (Bio-Rad) to amplify the target site and run under the conditions outlined in **Table 2**.

Primer	**Sequence**
MTWT1 (P1) (WT allele)	5’ – GAGGCTCAGACATATTGAAGA – 3’
MTWT2 (P2) (WT allele)	5’ – ACCAAATTGAAACTCGTTTTGATC – 3’
MTEOG (P3) (TRAF1 KO allele)	5’ – GCCCAATGCGAGCAGAAG – 3’
NeoS (P4) (TRAF1 KO allele)	5’ – CGACCACCAAGCGAAACAT – 3’

Table 1. *TRAF1 and WT genotyping primers.*

Temperature	**Time**	**Cycles**
95 °C	3 minutes	1
95 °C	15 seconds	35
53.5 °C	15 seconds	
72 °C	15 seconds	
72 °C	1 minute	1
4 °C	hold	

Table 2. *Thermo-cycler conditions for amplification of specific target sites for mouse genotyping.*

Next, both mixes containing the same genomic DNA but different primers were combined into a single 20 µL sample. The 20 µL mixes were fractioned on a 1% agarose gel for 90 minutes at 70 V. The genotype was verified using a gel imager to detect bands (**Figure 2**). A single band at size 1.2 kbp indicated the mouse expressed a homozygous TRAF1 KO genotype, a single band at size 1.4 kbp indicated the mouse is homozygous for the WT genotype, two visible bands indicated that the mice expressed a heterozygous genotype. Mice that were homozygous

for the TRAF1 KO and WT genotypes were used in subsequent experiments.

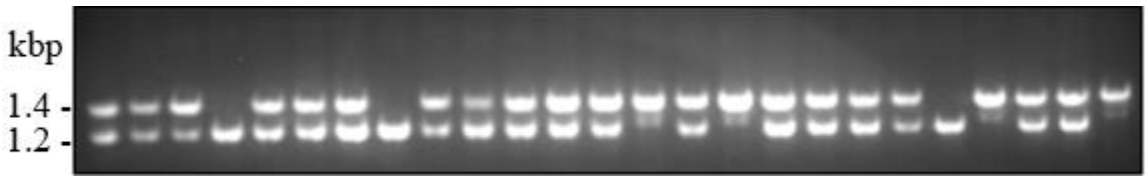

Figure 2. *Agarose gel image containing genotyping results of mice used in experiments.* Genomic DNA from tail clippings from C57BL/6 transgenic mice were amplified (Conditions in **Table 2**) using primers (**Table 1**) identifying the target sites for either TRAF1 KO or WT genotype. The resulting PCR products were loaded onto and fractioned on a 1% agarose gel for 90 minutes at 70 V and assessed with a gel imager. The data shown are representative of genotyping done of all mice used in experiments. A single 1.4 kbp band indicated WT genotype. A single 1.2 kbp band indicated TRAF1$^{-/-}$ genotype. Two bands indicated heterozygous genotype.

3.3 Mouse Bone Marrow Extraction

TRAF1$^{-/-}$ and WT mice were euthanized with 5% isoflurane (Fresenius Kabi) and sacrificed via cervical dislocation. For each mouse, both hind legs were carefully removed while ensuring that the femur and tibia were not broken. All tissue around the bones was removed and the bones were stored in RPMI media on ice until all samples were collected. In the biosafety cabinet, the bones were separated from each other at the knee joint and the tips of the bones were cut to expose the bone marrow. Using 10 mL of RPMI media (warmed to 37 ˚C) in a syringe with a 27-gauge needle, the contents of the bone marrow was flushed into a new 50 mL conical tube. 2.5 mL was used to flush each of the 4 bones. The solution was then spun down at 1500 RPM for 5 minutes at 4 ˚C. The pellet was resuspended in 2 mL of red blood cell lysing buffer (Sigma) and was incubated at room temperature for 5 minutes. Next, 10 mL of RPMI media was added on top of the cells in the lysis buffer and the mixture was centrifuged at 1500 RPM for 5 minutes at 4 ˚C. To resuspend the cell pellet, 40 mL of warmed RPMI media, containing 25% L-cell conditioned medium (LCM), was used to differentiate cells into bone marrow-derived

macrophages. The cells were then plated into 8 petri dishes, each containing 5 mL of media, and incubated for 3 days in a humidified incubator at 37 ˚C with 5% CO_2.

On day 3, the media (and cells that have not adhered to the bottom of the dish) from the first dish was aspirated without disrupting the cells that have adhered to the bottom of the plate. 3 mL of new RPMI media, warmed to 37 ˚C, was added to the dish and the cells were scraped carefully, but thoroughly, to lift the adhered cells off the dish and into suspension with the media. The media was then removed and placed in a new 50 mL conical tube. An additional 3 mL of media was added to the same plate to collect any excess cells; then swirled, aspirated, and placed into the second petri dish (with old media aspirated and discarded). The process was repeated for all eight dishes and resulted in a total volume of 24 mL of media with the undifferentiated bone-marrow macrophages in suspension. The cells were then counted using a hemocytometer and seeded at a concentration of 1.5×10^6 cells in 1 mL of RPMI media in each well of a 6-well tissue culture plate. The cells were then incubated again for 48 hours to proliferate and differentiate. By day 5, we had M0 (non-activated) bone-marrow derived macrophages ready for treatments.

3.4 Detection of IL-1β and Caspase-1 by Western Blot

3.4.1 Inflammasome Activation of Bone Marrow Derived Macrophages and THP-1 Cells

For examining the IL-1β and caspase-1 processing by western blot, murine bone marrow derived macrophages (on day 5) and PMA- differentiated THP-1 cells were primed with 100 ng/mL of LPS for 3 hours in RPMI media followed by 1 and 3 hours of stimulation with ATP (5 mM) and Nigericin (10 uM) in Opti-MEM I reduced serum media (Life Technologies). THP-1 cells used were seeded at 1.5×10^6 in 1 mL of RPMI media in a 6-well plate and differentiated with 100 nM PMA overnight before application of these treatments.

3.4.2 Immunoblotting

To concentrate proteins for analysis after cell stimulation, the supernatant of those cells was collected in 1.5 mL microcentrifuge tubes. Then, 100% Trichloroacetic acid (TCA) was added to each sample to bring the TCA concentration to 10%. Samples were vortexed for three-to-four seconds, followed by a 10-minute incubation on ice. Then samples were centrifuged for 10 minutes at 14.8 RPM at 4 °C, and the supernatant was then carefully removed leaving the protein pellet intact. Then, 45 uL of 1× Laemmli buffer was added to dissolve the protein pellet as the sample turned yellow in color. Hence, small amounts of 1 M NaOH were added until the color turned blue. The protein samples were then boiled at 95°C for 5 minutes.

Next, samples were loaded onto a 12% SDS-polyacrylamide gel to run at 60 V for 30 minutes followed by 120 V for 90 minutes. The protein samples were then transferred to a polyvinylidene difluoride membrane (Bio-Rad). Blots were blocked with 5% skim milk in TBST for 1 hour at room temperature. Then the membranes were probed with purified caspase-1 primary antibody (1:1000 dilution) (BioLegend 645102), and IL-1β primary antibody (1:1000 dilution) (R & D systems MAB601-SP), and incubated overnight at 4 °C. Subsequently, the membranes were incubated with peroxidase-conjugated secondary antibodies anti-rat (1:10,000) for detection of caspase-1, and anti-goat (1:10,000) for detection of IL-1β for 1 hour at room temperature. Immunoreactive proteins were detected with Immobilon Forte (Millipore) western blotting detection reagent using ChemiDoc MP imaging system (Bio-Rad).

3.5 MSU-induced Peritonitis Mouse Model

3.5.1 Injection and Lavage

A previously described protocol of inducing inflammasome-dependent peritonitis in mice using mono sodium urate (MSU) crystals was used[53]. A synopsis of the protocol is as follows;

TRAF1$^{-/-}$ and WT mice between 6-8 weeks of age were injected interperitoneally with 180 μL of phosphate buffered saline without calcium or magnesium chloride (PBS -/-) (Sigma) or MSU crystals suspended in sterile PBS -/- at a concentration of 5 or 10 mg/mL. All mice used were age and sex matched. Within each treatment condition, as many littermates as possible were used to minimize variation between the mice used; in all of experiments conducted, we were able to achieve this in all groups except for a few instances. The mice were then anesthetized using 5% isoflurane (Fresnius Kabi) and sacrificed via cervical dislocation either 4, 8 or 16 hours after the initial injection. The skin of the belly was then opened without disrupting the peritoneum and 3-5 mL of PBS -/- was injected into the peritoneal cavity. Following shaking the mouse, the PBS -/- was aspirated from the cavity, placed into 15 mL conical tubes, and spun down to pellet the cells recovered from the peritoneum. The supernatant was taken and frozen at -80 ˚C for later analysis of IL-1β secretion via enzyme linked immunosorbent assays (ELISA). The cells were immediately prepared for analysis via flow cytometry. Using flow cytometry, we assessed the amount of inflammation that had occurred by evaluating the number of neutrophils, monocytes, resident macrophages and monocyte-derived macrophages present in each sample.

3.5.2 Flow Cytometry

Once all samples from the MSU-induced peritonitis mouse model were spun down and collected, they were resuspended in 1 mL of 1× red blood cell lysis buffer that had been diluted from a 10× stock solution (ThermoFisher Scientific). The samples were then incubated at room temperature for 5 minutes. Once complete, 5 mL of PBS -/- was added onto each sample and spun down at 1200 RPM for 3 minutes at 4 ˚C. The supernatant was aspirated and discarded, and the cells were resuspended in 300 μL of FACS buffer (PBS -/- with 2% FBS) and kept on ice. 15 μL of each sample was taken and mixed into one well of a 96-well, round-bottom plate to be

used as an unstained control. The remaining 285 μL from each sample was added to additional wells of the same plate. The plate was then be centrifuged at 1200 RPM for 3 minutes at 4 ˚C. Next, cells were resuspended in 50 μL of CD16/CD32 mouse monoclonal antibody (ThermoFisher Scientific,) diluted 1:25 with FACS buffer. This antibody was used to block Fc receptors on cells in the samples to increase the specificity of the antibodies used next. The unstained well was resuspended in FACS buffer. The plate was then incubated at 4 ˚C for 10 minutes. Following this, the plate was centrifuged again and cells were resuspended in a prepared staining mix containing LIVE/DEAD Fixable Aqua Dead Cell Stain (), CD45 (), LY6G (), F4/80 (), and CD11b () mouse monoclonal antibodies, and superbright staining buffer () to prevent non-specific polymer interactions (all from ThermoFisher Scientific). Antibody and dye information are described in **Table 3**. Once again, the unstained well was resuspended in FACS buffer. The plate was protected from light and incubated for 30 minutes at 4 ˚C. Once complete, 200 μL of FACS buffer was added on top of each sample and the plate was centrifuged at 1200 RPM for 3 minutes at 4 ˚C. The supernatant was aspirated and discarded, then the samples were washed two more times. Afterwards the cells were resuspended in an additional 200 μL of FACS buffer and the plate was loaded into the Attune NxT Flow Cytometer (ThermoFisher Scientific).

Target (Antigen/Membrane Property)	Fluorophore	Laser	Channel
CD11b	Super Bright 780	Violet 405 nm	780/60
CD45	FITC	Blue 488 nm	530/30
F4/80	APC-eFluor 780	Red 637 nm	780/60
Ly-6G	Super Bright 600	Violet 405 nm	610/20
Compromised membrane (Free amines) (LIVE/DEAD Fixable Aqua Dead Cell Stain)		Violet 405 nm	525/50

Table 3. *Fluorescence information for antibodies and dye used to identify target cells via flow cytometry.*

The first time running this assay, a compensation was performed to correct for fluorescent spill-over into other detectors in the machine and prevent cells stained with a single antibody to appear as double positive. To do this, half of a drop of compensation beads was added to 4 wells of a 96-well plate. Each drop had one of CD45, LY6G, F4/80, or CD11b mouse monoclonal antibodies added to it. Then the beads incubated and were treated as described above. A small number of cells were also taken from samples and had 100% ethanol applied to them for 5 minutes before being spun down and subsequently treated like the unstained sample described above. This sample was stained with aqua fluorescent reactive dye only to provide a compensation for the live/dead cell stain. These 5 conditions ran as a compensation in the flow cytometer and the settings were automatically corrected by the software for analysis of the fully treated and stained samples.

Leukocytes were identified $CD45^{+}$. Neutrophils were identified as $CD11b^{+}$ $Ly6G^{+}$, while monocytes and macrophages were first gated on $CD11b^{+}$ $Ly6G^{-}$ then monocytes were identified as $F480^{lo}$, monocyte-derived macrophages as $F4/80^{int}$, while resident peritoneal macrophages as $F4/80^{hi}$. **Figure 3** is a representative example of the gating strategy used identify cells of interest.

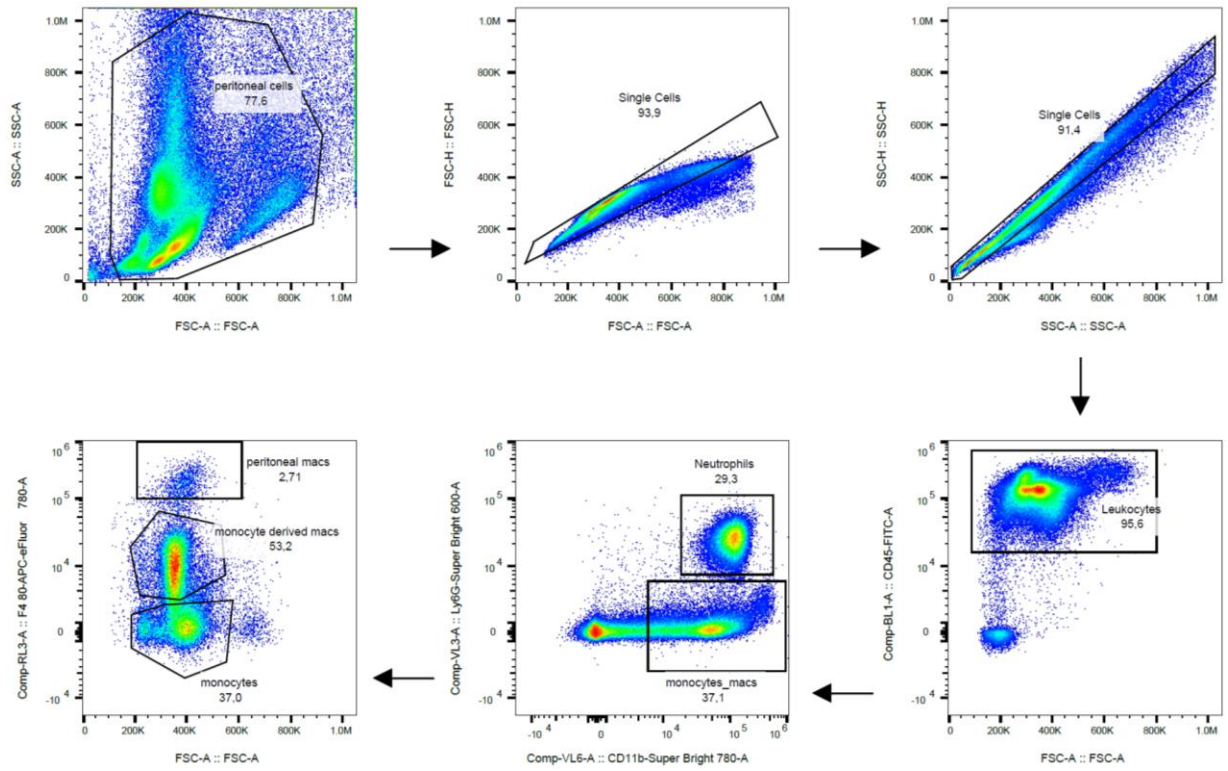

Figure 3. *Gating strategy for flow cytometry analysis of MSU-induced peritonitis.* Once cells were stained and washed with FACS buffer, they were loaded into the flow cytometer. After running the compensation, the unstained sample was run to ensure the majority of the cells were located in the middle of each plot. The above gating strategy was used to exclude debris, doublets, and dead cells from subsequent analysis. Then gates were used to identify specific leukocytes (neutrophils, monocytes, and macrophages) based on their antibody staining. This strategy is representative of what was used for all flow cytometry experiments conducted.

3.6 Crystal-induced Arthritis

3.6.1 Injection Protocol

In collaboration with a postdoctoral lab member specialized in animal intraarticular injections and surgery (Ali Mirzaesmaeili), 500 µg of MSU crystals suspended in 10 µL of PBS -/- or 300 µg (MSU condition), MSU crystals suspended in 10 µL of 0.5 mM palmitic acid (PA) (MSU + PA condition) or PBS -/- alone (PBS condition) was injected into the hind leg knee joints of WT and TRAF$^{-/-}$ mice. Mirzaesmaeili conducted the interarticular injections and dissection of the synovium following disease progression. 20 12-week-old male mice were used,

including 11 TRAF1$^{-/-}$ mice and 9 WT mice. The injections occurred over two days; 5 TRAF1$^{-/-}$ mice and 5 WT mice received MSU + PA injections on the first day and 6 TRAF1$^{-/-}$ mice along with 4 WT mice received MSU injections on day 2. All MSU and MSU + PA injections were made into the left knees of the mice, and 4 mice from the WT and TRAF1$^{-/-}$ (2 from each condition on each day) conditions were also injected with PBS -/- in the right knees for use as controls.

To make the injections, isoflurane anaesthesia was induced and maintained between 2% and 5%. Anesthesia was confirmed by checking the animal's lack of response to a pinch stimulus on the hind paws. Each mouse was placed in dorsal recumbency. The surgical field was washed and disinfected with 7.5% povidone-iodine. The scrub solution was washed off with 70% isopropyl alcohol, each mouse was transferred to the microsurgical operating room and the final preparation solution of 10% povidone-iodine was applied. A 30-gauge needle attached to a syringe was inserted posterior to the medial edge of the patellar ligament, through the triangle formed by the epicondyle of the femur, the meniscal/tibial plateau. To find the precise site of injection, a 26 G needle attached to a syringe was run horizontally along the knee until the gap beneath the patella could be found. The area was marked by applying gentle pressure and lifting the needle and syringe (Hamilton syringe gauge 30) vertically for the injection. The needle was inserted into the marked area through the patellar tendon perpendicular to the tibia and the treatment solution was injected.

3.6.2 Tissue Extraction

Following injections, my role was to record macroscopic joint swelling before, as well as 2 and 4 hours after injection by a caliper. Then, the mice were anesthetized with 5% isoflurane and euthanized via cervical dislocation 4 hours after being injected. The joints of each mouse

were photographed before the synovia were isolated by the postdoctoral member of our lab. Once isolated, each synovium was cut in half; one half was analyzed for IL-1β secretion by ELISA and the other half was used for RNA extraction. The RNA extracted from the other half was used to make complimentary DNA via reverse transcription and then gene expression of targets like *IL-1β, IL-6, TNFα* and *NLRP3,* were assessed using real-time polymerase chain reaction (PCR) (Full list of primers used and genes analyzed are in **Table 7**).

3.6.3 RNA Extraction

The Ambion RNAqueous-Micro Micro Scale RNA Isolation Kit (ThermoFisher Scientific) was used to isolate RNA from the synovium extracted from the mice that have undergone interarticular injections. The pieces of synovium that were cut in half weighed between 0.1 and 0.3 mg and required a specialized kit specifically designed for optimal RNA extraction from micro-dissected tissue. To begin the procedure, samples were removed from storage at -80 ˚C and immediately immersed in 100 μL of lysis solution that contained guanidinium thiocyanate, a strong chaotropic agent that disrupts cell membranes and rapidly inactivates ribonucleases. Using a hand-held homogenizer, each synovium sample was disrupted for about 2 minutes in a 1.5 mL microcentrifuge tubes containing the lysis solution. The lysate was then mixed with 50 μL of 100% ethanol and vortexed briefly, but thoroughly. Next, the lysate/ethanol mixture was applied to a small silica-based filter that selectively binds RNA and allowed for elution in small volumes (10-20 μL) so that the acquired RNA solution was more concentrated than that obtained from standard RNA extraction kits. The filter cartridge was inserted into a collection tube and centrifuged (all centrifugation steps performed at 16,500 g) for about 30 seconds. The RNA, now bound to the filter, was washed 3 times with 180 μL of the wash solutions (with required amount of ethanol added) included in the kit. After the addition of

each wash solution, the samples were centrifuged for about 10 seconds. Once the third wash was completed, the flow-through was discarded and the samples were spun-down once again for 1 minute to remove residual fluid and dry the filter. The filter cartridge was then replaced with a new one and the samples were eluted with 7.5 µL of the provided elution solution that was pre-heated to 75 ˚C. After incubating for 1 minute at room temperature, the samples were spun down for 30 seconds to elute the RNA. Following this, an additional 7.5 µL of pre-heated elution solution was added, incubated for 1 minute and spun down to elute the RNA once again. The resulting 15 µL of RNA-elution solution was then prepared to make complimentary DNA via reverse transcription.

3.6.4 Formation of Complimentary DNA (cDNA) via Reverse Transcription

For each sample, 14.8 µL of the RNA obtained from the RNA extraction was combined with 1 µL of Oligo dT and 1 µL of 10 mM dNTP (16.8 µL final volume). The samples were placed in a thermo-cycler according the conditions outlined below in **Table 4**. Once the protocol was complete, 0.2 µL of RNAse inhibitor, 1 µL of M-MuLV Reverse Transcriptase and 2 µL of 10× reverse transcriptase buffer was added to each sample. The samples were then placed in the thermo-cycler again and run according to the protocol outlined in **Table 5**. Once completed, the acquired 20 µL of cDNA was stored at -20 ˚C until analysis via real-time PCR.

Step	**Temperature**	**Time**
1	65 ˚C	5 minutes

Table 4. *Thermo-cycler conditions for reverse transcription step 1.*

Step	Temperature	Time
1	37 ˚C	50 minutes
2	72 ˚C	15 minutes
3	4 ˚C	Infinite hold

Table 5. *Thermo-cycler conditions for reverse transcription step 2.*

3.6.5 Real-Time PCR

The acquired cDNA was thawed and diluted 1:5 using RNAse and DNAse free water. Of this diluted cDNA, some of the sample was removed and further diluted 1:10 in RNAse and DNAse free water to achieve a 1:50 diluted final sample of cDNA. 4 μL of the diluted cDNA was added to 6 μL of a prepared mix containing 0.6 μL of the forward and reverse primer (10 mM concentration) of the gene of interest (**Table 7**) and 5.5 μL of 2× SYBR Green PCR Master Mix (Thermo Fisher Scientific). Each sample was loaded into a 384-well plate and run according to the conditions outlined in **Table 6**. All primers were validated, either in previous work from other lab members or by myself.

The resulting quantitation cycle (Cq) values, which represent the number of cycles required for each sample to emit a fluorescent signal that can be detected by the machine, were normalized to the housekeeping gene, *RPLP0.* This was done by subtracting the Cq values of the samples targeting *RPLP0* from the Cq values of the samples containing the gene targets of interest in the same treatment conditions, denoted as ΔCq. Next, the average of the ΔCq values of the samples containing the cDNA from synovium of the PBS controls was subtracted from the ΔCq values of each sample treated with MSU or MSU + PA, denoted as ΔΔCq. Fold changed with respect to results from PBS controls was then calculated as $2^{-\Delta\Delta Cq}$.

Step	Temperature	Time	Notes
1	95 ˚C	30 seconds	
2	95 ˚C	10 seconds	40 Cycles
3	60 ˚C	30 seconds	
4	Fluorescence Measurement		
5	95 ˚C	10 seconds	
6	65 ˚C	31 seconds	
7	65 ˚C + 0.5 ˚C/cycle	5 seconds	61 Cycles
8	Fluorescence Measurement		

Table 6. *Real-time PCR conditions for analysis of gene expression of cDNA created from samples of dissected synovium.*

Primer	Target Gene	Sequence
mRPLP0 For	*RPLP0*	5’ – TTGGAGTGACATCGTCTT – 3’
mRPLP0 Rev		5’ – ATCTTGAGGAAGTAGTTGGA – 3’
mMCP5 For	*MCP5*	5’ – TGGTTCCTGACTCCTCTA – 3’
mMCP5 Rev		5’ – TGCTTGTGATTCTCCTGTA – 3’
mIL-1b For	*IL-1β*	5’ – GCAGCACATCAACAAGAG – 3’
mIL-1b Rev		5’ – CAGCAGGTTATCATCATCATC – 3’
mIL6 For	*IL-6*	5’ – ACAGAAGGAGTGGCTAAG – 3’
mIL6 Rev		5’ – AGAGAACAACATAAGTCAGATAC – 3’
mCxcl10 For	*CXCL10*	5’ – ATTCTTTAAGGGCTGGTCTGA – 3’
mCxcl10 Rev		5’ – CACCTCCACATAGCTTACAGT – 3’
mTNFa For	*TNFα*	5’ – AGAATGAGGCTGGATAAGAT – 3’
mTNFa Rev		5’ – GAGGCAACAAGGTAGAGA – 3’

mIL18 For	*IL-18*	5’ – GCTGTGACCCTCTCTGTGAA – 3’
mIL18 Rev		5’ – GGCAAGCAAGAAAGTGTCCT – 3’
mCaspase-1 For	*Caspase-1*	5’ – AGATGCCCACTGCTGATAGG – 3’
mCaspase-1 Rev		5’ – TTGGCACGATTCTCAGCATA – 3’
mNLRP3 For	*NLRP3*	5’ – GTGGTGACCCTCTGTGAGGT – 3’
mNLRP3 Rev		5’ – TCTTCCTGGAGCGCTTCTAA – 3’
mASC For	*PYCARD* (ASC)	5’ – CCAGTGTCCCTGCTCAGAGT – 3’
mASC Rev		5’ – TCATCTTGTCTTGGCTGGTG – 3’
mAim2 For	*AIM2*	5’ – ACAAAGTGCGAGGAAGGAGA – 3’
mAim2 Rev		5’ – TTTGGCTTTGCAGCCTTAAT – 3’
mS100A8 For	S100A8	5’ – TGCCCTCTACAAGAATGACT – 3’
mS100A8 Rev		5’ – AAGCTCTGCTACTCCTTGTG – 3’
mS100A9 For	S100A9	5’ – CGACACCTTCCATCAATACT – 3’
mS100A9 Rev		5’ – TCAGCATCATACACTCCTCA – 3’

Table 7. *Primers used for analysis of respective gene expression.*

3.7 IL-1β ELISA

The IL-1β mouse uncoated ELISA kit (Invitrogen) was used to perform quantitative ELISA to detect and quantify protein levels of IL-1β in the supernatant of previously homogenized synovia, immune cells collected from peritoneum of mice, and treated murine bone-marrow derived macrophages. First, the anti-mouse IL-1β capture antibody (100 μL/well) was immobilized on high protein-binding ELISA 96-well plates (Greiner bio-one) by overnight incubation at 4°C. Then the wells were aspirated and washed three times with wash buffer consisting of PBS with 0.05% Tween. For each wash, and all subsequent ones, the wash solution soaked for about 1 minute before being aspirated. The plate was blocked with 200 μL of 1× ELISA/ELISPOT diluent to prevent nonspecific binding and incubated for 1 hour at room

temperature. Again, the plate was aspirated and washed three times with the wash buffer. The protein standard provided in the kit was used to make a standard curve of 15-1000 pg/mL by performing a 2-fold serial dilution in the 1× ELISA/ELISPOT diluent. 100 µL of supernatant and the prepared standards were added to the plate and incubated overnight at 4°C. Before being added to the plate, supernatant of the murine bone marrow derived macrophages treated with nigericin and ATP was diluted 1:50 and 1:10 in 1× ELISA/ELISPOT diluent, respectively. The next day, the plate was aspirated and washed five times, followed by the addition of 100 µL/well of biotin-conjugated anti-mouse IL-1β antibody for 1 hour at room temperature. The plate was then aspirated and washed five times. The Avidin-horseradish peroxidase (HRP) conjugate (100 µL/well) was added next to the plate and incubated for 30 minutes at room temperature. The plate was aspirated and washed seven times prior to the addition of 100 µL of 1× Tetramethylbenzidine (TMB), the substrate for HRP, followed by a 15-minute incubation. Lastly, 100 µL/well of 1 M phosphoric acid, the stop solution, was added to each sample and absorbance was measured at 450 nm and 570 nm. The values of 570 nm are subtracted from those of 450 nm and the data was analysed. To analyze the data, the results of the subtracted absorbance for all samples were averaged between the two duplicates and then standardized by subtracting each of these values by the absorbance reading of the blank sample. Then, using a standard curve made from the results of the standards provided with the kit, the concentration of IL-1β was calculated. If samples were diluted, the results were multiplied by their respective dilution factor.

3.8 CRISPR/Cas9 HDR-mediated Knock-in Detection in Single-Clones of THP-1 Cells

3.8.1 Creation of THP-1 Cells with TRAF1 V203A Mutation

Another member of our lab (Safoura Zangiabadi) used CRISPR/Cas9 to create a homology-directed repair (HDR) mediated knock-in of the V203A mutation in a bulk population of WT THP-1 human monocytic leukemia cells obtained from Sigma-Aldrich. The bulk-edited population of THP-1 V203A cells were counted using a hemocytometer and diluted to a concentration of 0.5-1 cells/100 μL of media, which yielded 1 cell per well in most wells of a 96-well flat bottom plate. The single cells were kept in an incubator at 37 °C for clonal expansion for 2-8 weeks. The plates were screened regularly to monitor the growth of the cell colonies using a microscope. When colonies reached 70% confluency, they were transferred into a 24-well plate and topped up with fresh RPMI media. Once the successful individual clones expanded, they were isolated and analyzed for successful insertion of mutants using the Guide-it Knock-in Screening Kit (Takara Bio).

3.8.2 Detection of Successful TRAF1 V203A Mutation

The Guide-it Knock-in Screening Kit was used to screen for a successful homology-directed repair and a detection of our desired single-nucleotide substitutions (V203A) in the single-clones of THP-1 cells that had been previously prepared by another member of our lab. The enzymatic assay is based on the capacity of provided Guide-it Flapase to recognize and cleave a specific tripartite structure formed by the target site and the two designed oligo probes. These flap probes, as well as the displacement, and control oligos (60-90 bp in length) were designed by our lab based on the target sequence encoding the wild-type and mutated sequence according to the manufacturer's primer design tool (**Table 8**). The displacement oligo hybridizes the PCR product 3' relative to the interrogated base and has an extra noncomplementary base at

its 3’ end. The flap-probe oligo encodes the sequence we wanted to detect and one of two fixed, noncomplementary sequences at its 5’ end that triggers the generation of either green or red fluorescence by the Guide-it Flap Detector. Following the enzymatic assay, the kit allows for the detection of clonal heterozygosity with green or red fluorescence corresponding to the presence of SNP or wild-type alleles, respectively.

Primer Name	**Primer Sequence 5’-3’**	**Annealing temperature (Ta)**
V203A SNP Control Oligo	AGGCCTCCACCTCCTTGTTGAGGGCAGCAACA ATGTTCTCAAACACACGCAGCTTCCC	63°C
V203A WT Control Oligo	AGGCCTCCACCTCCTTGTTGAGGACAGCAACA ATGTTCTCAAACACACGCAGCTTCCC	63°C
V203A Displacement	CTGCGTGTGTTTGAGAACATTGTTGCTGA	63°C
V203A Flap probe SNP	ACGGACGCGGAGCCCTCAACAAGGAGGTG/3C6/	63°C
V203A Flap probe WT	AGGCCACGGACGTCCTCAACAAGGAGGTG/3C6/	63°C

Table 8. *List of designed primers for CRISPR/Cas9 HDR-mediated knock-in screening.*

3.8.2.1 Cell Lysis

Once the cells in the 24-well plate reached 70% confluency, they were counted using a hemocytometer. The volume of media containing 2×10^5 cells was removed from each well and placed into 1.5 mL microcentrifuge tubes. The cells were then spun down at 300 g for 5 minutes at 4 ˚C. Supernatant was discarded and the cell pellet was washed twice with 100 µL of PBS -/-. After the second wash, the PBS supernatant was aspirated and discarded, and the cells were

resuspended in 50 μL of MightyPrep Reagent to extract DNA and transferred to a 96-well PCR plate. The plate was then covered and placed in the thermo cycler for 10 minutes at 95 ˚C. Following this, the plate was centrifuged for 10 minutes at 1200 g. 45 μL of the supernatant was removed without disrupting the pellet that has formed and stored at -20 ˚C until the next step.

3.8.2.2 Amplification of Target Site

To amplify the target site of the HDR mediated knock-in, a PCR reaction mixture was composed according to the **Table 9**.

Reagent	**Volume for 1 sample (μL)**	**Volume for 110 samples (μL) ***
2× Reaction Buffer	12.5	1,512.5
RNase Free Water	8.5	1,028.5
Forward Primer (10 mM)	0.75	90.75
Reverse Primer (10 mM)	0.75	90.75
Polymerase	0.5	60.5
Total Volume	23.0	2783

Table 9. *Components of reaction mixture used to amplify target site that will be screened for the V203A mutation.*

*Volume includes additional ~10% to account for pipetting errors.

23 μL of the prepared mixture was added into 110 wells over two 96-well PCR plates. The previously prepared PCR products were then thawed on ice. 2 μL of each was added to its corresponding well in the PCR plates with 23 μL of the reaction mixture and was mixed briefly by pipetting up and down. The plates were then covered and centrifuged at 700 g for 1 minute at 4 ˚C. The plates were then be loaded into two thermo cyclers and ran according to the **Table 10**.

Temperature	Time	Cycles
98 ˚C	2 minutes	1
98 ˚C	10 seconds	35
68 ˚C	1 minute	
4 ˚C	Hold	

Table 10. *Thermo-cycler conditions for amplification of target site.*

Next, 3 µL of the DNA amplification products from the PCR reaction was mixed with 10 µL of deionized water and fractioned on a 2% agarose gel for 90 minutes at 70 V. The PCR product was verified using a gel imager to detect a single band of correct size. The remaining product was stored at -20 ˚C until the following steps.

3.8.2.3 Enzymatic Assay

The PCR product from the previous step was diluted 1:40 with dilution buffer provided in the Guide-it Knock-in Screening Kit (2 µL of each sample will be added to 78 µL of the buffer). Then, previously designed WT and SNP control oligos, displacement oligos, and flap-probe oligos were resuspended in RNAase-free water to achieve a final concentration of 1 nM, 1 µM, and 20 µM, respectively. Next, a heterozygous positive control was prepared by mixing WT and SNP control in equal volume for a final concentration of 0.5 nM. In a 384-well plate, 10 µL of WT, SNP control oligo, heterozygous positive control, and water (non-template control) were pipetted per well in duplicate. 10 µL of each diluted PCR product was also added to their respective wells in duplicate as well. Next, an annealing master mix (**Table 11**) was prepared in a 1.5 mL microcentrifuge tube. Then, 5 µL of the prepared annealing master mix was added to each well containing the aforementioned samples and controls. 15 µL of Guide-it Knock-in positive control mix and Guide-it Knock-in negative control mix that were provided in the kit

were also added to separate wells in duplicate to serve as additional controls. The plate was then sealed and centrifuged at 700 g for 1 minute. The plate was then be loaded into a real-time PCR machine (Bio-Rad) to anneal the WT and SNP control oligos with the displacement and flap-probe oligos. The protocol ran as described in **Table 12**.

Reagent	**Volume for N samples (µL)**	**Volume for Samples Described (µL) ***
Annealing Buffer	2.0 × N	500.0
Flap-probe oligo SNP [20 µL]	0.5 × N	125.0
Flap-probe oligo WT [20 µL]	0.5 × N	125.0
Displacement oligo [1 µM]	1.0 × N	250.0
RNAse-free Water	1.0 × N	250.0
Total Volume	5.0	1250.0

Table 11. *Contents of mixture prepared for annealing reaction necessary for screening.*

*Volume includes amount of master mix required for 110 samples and 4 controls, all in duplicate and with additional ~10% to account for pipetting error.

Temperature	Time
95 ˚C	5 minutes
95 ˚C	Step-down at 0.1 ˚C per second
63 ˚C	
63 ˚C	10 minutes
63 ˚C	Hold

Table 12. *Thermo-cycler conditions for annealing step.*

3.8.2.4 Enzymatic Reaction

While the annealing step occurred, an enzymatic reaction master mix was prepared as described in **Table 13**.

Reagent	Volume for N samples (µL)	Volume for Samples Described (µL) *
Flapase Buffer	3.0 × N	750.0
Guide-it Green Flap Detector	0.5 × N	125.0
Guide-it Red Flap Detector	0.5 × N	125.0
Guide-it Flapase	1.0 × N	250.0
Total Volume	5.0	1250.0

Table 13. *Contents of master mix prepared for enzymatic reaction for screening.*

*Volume includes amount of master mix required for 110 samples and 4 controls, all in duplicate and with additional ~10% to account for pipetting error.

In a new 384-well plate, 5 µL of the enzymatic reaction master mix was then pipetted into the same wells as the annealing reactions plate previously prepared. Then the contents of the previously-ran 384-well plate were transferred to the plate containing the enzymatic reaction master mix. The plate was sealed and centrifuged at 700 g for 1 minute. Lastly, the plate was

placed in a real-time PCR machine to read green and red fluorescence. The plate was kept at 63°C for 75 minutes followed by green and red fluorescent measurements.

To verify the V203A mutation, samples of the amplified PCR product obtained in the previous step was sent to The Centre for Applied Genomics (TCAG) DNA/Sequencing Facility, operated by The Hospital for Sick Children (SickKids). The expanded single-cell clones (still in 24-well tissue culture plate) that were detected to be homozygous knock-ins were expanded to a 6-well tissue-culture plate, then T25 flask, and eventually to a T75 flask.

3.9 Detection of NF-κB Activation by Western Blot

3.9.1 LPS Treatment of THP-1 Cells

To examine the extent of NF-κB activation and production of components required for inflammasome formation following signal 1, cells were treated with 1 μg/mL of LPS in RPMI media for 15 and 30 minutes, and 1, 3, and 6 hours. THP-1 cells used were seeded at 1.5×106 in 1 mL of RPMI media in a 6-well plate overnight before application of the treatments.

Once treatments on THP-1 cells were completed, all the cells in suspension were aspirated and placed into 1.5 mL microcentrifuge tubes and centrifuged at 1000 g for 5 minutes at 4 °C. The supernatant was aspirated and discarded, and the cells were resuspended in 1 mL of ice-cold PBS. The cells were once again centrifuged at 1000 g for 5 minutes at 4 °C. Supernatant was once again aspirated and discarded and the cell pellet was resuspended in 100 μL of freshly prepared 1× lysis buffer containing 1% NP- 40 (Igepal CA-630), 100mM Tris pH 8.0, 20% glycerol, 0.2mM EDTA, 150mM NaCl, cOmplete™, Mini, EDTA-free Protease Inhibitor Cocktail (Sigma-Aldrich), 1× Phosphatase Inhibitor Cocktail 3 (Sigma-Aldrich), 1 mM DTT (Sigma-Aldrich) and deionized water. The lysates were kept on ice and vortexed every 5 minutes

for total 30 minutes to ensure cell lysis. The lysates were centrifuged at 14.8 RPM at 4 °C for 15 minutes and the supernatant was collected in pre-chilled new 1.5 mL microcentrifuge tubes. The amount of protein concentration was measured in the lysate using the Bradford Reagent (BioRad).

3.9.2 Bradford Protein Assay

The Bradford protein assay was used to determine the protein concentration of the samples. The Bradford assay was performed in a 96-well flat bottom plate. The Bradford Reagent (1×) was removed from the 4 °C storage and let reach room temperature. Bovine serum albumin (BSA) was also removed from -20 °C and let thaw on ice. BSA (1 mg/mL) was used as a standard protein to perform a two-fold serial dilution. This was performed by preparing 7 protein standards including 128 µg/mL, 64 µg/mL, 32 µg/mL, 16 µg/mL, 8 µg/mL, 4 µg/mL, and 2 µg/mL. The 128 µg/mL of the standard was prepared in a 1.5 mL microcentrifuge tube by adding 872 µL of the 1× Bradford reagent and 128 µL of the BSA (1 mg/mL). The mixture was vortexed and 500 µL was transferred into the next microcentrifuge containing 500 µL of the reagent to make a final concentration of 64 µg/mL. The serial dilution continued until the lowest concentration of 2 µg/mL was achieved. The reagent alone was used as a blank for background subtraction. The samples were prepared by adding 5 µL of each sample in a 96-well flat bottom plate followed by addition of 195 µL of the 1× Bradford reagent to achieve a 1:40 dilution of the protein samples. The samples and the reagent were mixed in wells of a flat-bottom 96 well plate by pipetting and the absorbance was measured after 5 minutes at 595 nm using a plate reader (Verioskan). The concentrations of the unknown protein samples were calculated by plotting a BSA standard curve. The line of best fit and the equation for the standard curve was used to

calculate the samples' protein concentrations and ensure equal amounts of protein were loaded for analysis via western blot.

3.9.3 Immunoblotting

The protein samples were eluted with 5× Laemmeli Sample Buffer (BioRad) with 2-ME and deionized water to achieve a 1× final protein concentration. The protein samples were heated at 100°C for 5 minutes and loaded onto a 10% SDS-polyacrylamide to run for 60 V for 30 minutes followed by 120 V for 90 minutes. Then the protein samples were transferred to a polyvinyldene difluoride membrane (Bio-Rad). The blot was blocked with 5% skim milk in TBST for 1 hour at room temperature. The membranes were incubated with phospho-IκBα (Cell Signaling, 2859S), IκBα (Cell Signaling, 4814S), IL-1β (R&D Systems Inc. MAB8929), and cleaved caspase-1 (Cell Signaling, 4199S) primary antibodies (1:1000) overnight on successive nights at 4 °C and β-actin primary antibody (Invitrogen, MA5-15739) (1:1000) for 1 hour at room temperature. Following incubation with the primary antibodies, the membranes were incubated with peroxidase-conjugated secondary antibodies (1:10,000 dilution) for 1 hour at room temperature for detection. Anti-rabbit was used for detection of phospho- IκBα and cleaved caspase-1, anti-mouse for IκBα and β-actin, and anti-goat for IL-1β. Immunoreactive proteins were detected with Immobilon Forte (Millipore) and SuperSignal West Pico PLUS (ThermoFisher Scientific) western blotting detection reagents using ChemiDoc MP imaging system (Bio-Rad).

3.10 Statistical Analysis

Groups were compared for significance using two-way ANOVA (two-tailed) and Šídák's multiple comparison test by GraphPad Prism 4.0. A $p<0.05$, $p<0.01$, and $p<0.001$ were considered as significant. Data are reported as mean ± SEM.

Chapter Four: Results

4.1 TRAF1 Inhibits NLRP3 Inflammasome Activation in-vivo

4.1.1 Protein Expression

To begin, we needed to determine if the previous results outlining TRAF1's inhibition of NLRP3 inflammasome activation in-vitro also occurred in-vivo. To do so, macrophages derived from the bone marrow of TRAF1-/- and WT mice were obtained. Once plated, the cells were treated with LPS for 3 hours to prime the cells and initiate signal 1 of NLRP3 inflammasome activation. Following this, cells were treated with either ATP or nigericin for 1 or 3 hours to initiate signal 2 and full NLRP3 inflammasome activation. One sample of each of the TRAF1-/- and WT derived macrophages was left untreated and one was treated with LPS alone. Once treatments concluded, the proteins present in the supernatant of the cells were precipitated and the expression of caspase-1 and IL-1β were quantified via western blot. These were analyzed because the mature forms of these three proteins are secreted downstream of NLRP3 inflammasome activation. **Figure 4** indicates the results of the protein quantification.

Figure 4 displays the 45-kDa pro-caspase-1 and the 20 kDa P20 subunit of active caspase-1. As demonstrated in the western blot, there was increased processing of caspase-1 upon stimulation with the NLRP3 inducers nigericin and ATP, in $TRAF1^{-/-}$ mice compared to WT mice as indicated by the intensity of the bands. The expression of caspase-1 was more robust upon stimulation with nigericin than ATP. These results demonstrated that TRAF1 reduces caspase-1 processing in WT controls compared to $TRAF1^{-/-}$ mice.

Figure 4 also indicates that the 37 kDa pro-IL-1β was proteolytically cleaved into the bioactive 17 kDa mature IL-1β form. The western blot analysis shows increased processing of IL-1β upon stimulation with the NLRP3 inducers, nigericin and ATP, in $TRAF1^{-/-}$ mice

compared to WT mice, as indicated by the intensity of the bands. The expression of mature IL-1β was more robust upon stimulation with nigericin than ATP. These results are indicative of TRAF1 reducing processing and secretion of IL-1β in WT controls compared to TRAF1$^{-/-}$ mice.

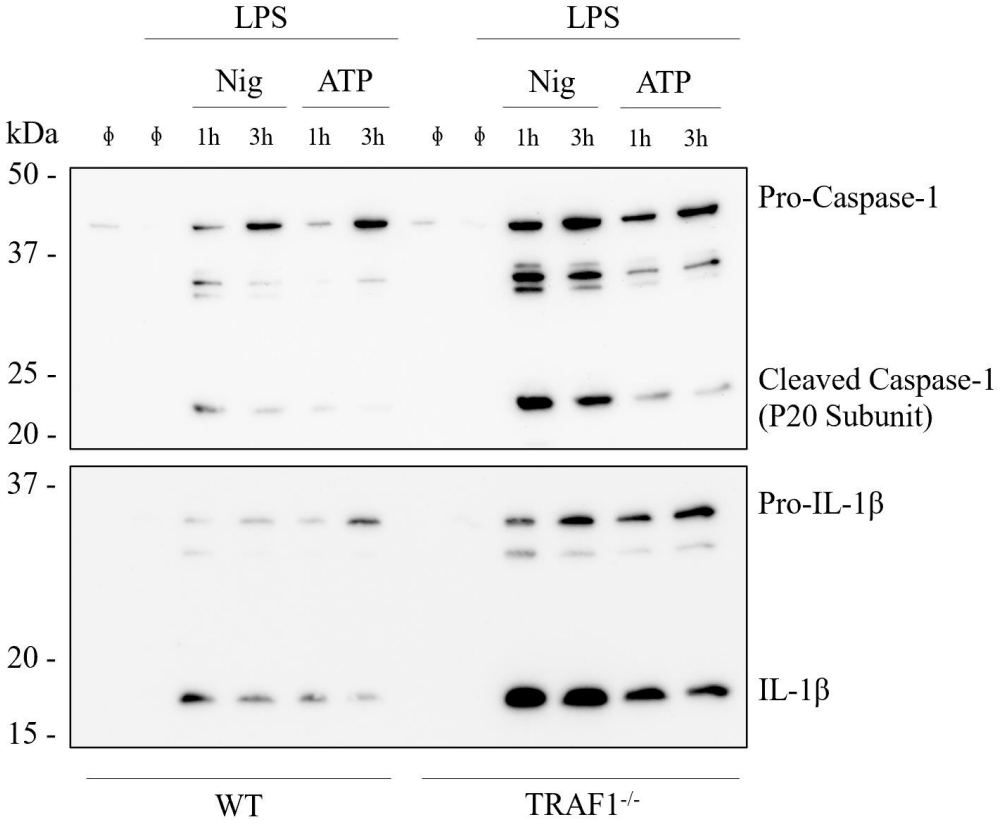

Figure 4. *Caspase-1 and IL-1β processing in macrophages derived from bone marrow of TRAF1$^{-/-}$ and WT mice.* Bone marrow derived macrophages from TRAF1$^{-/-}$ and WT mice were treated with LPS (100 ng/mL) for 3 hours prior to stimulations with ATP (5 mM) and Nigericin (10 µM) for 1 and 3 hours. The culture supernatants were collected, the proteins in the supernatant were precipitated using 100% TCA and immunoblotted for expression of cleaved and uncleaved caspase-1, as well as cleaved and uncleaved IL-1β. The data shown are representative of four independent experiments.

4.1.2 Mouse IL-1β ELISA

To further assess the role of TRAF1 in inflammasome activation, some supernatant collected from the above experiments was reserved for analysis of IL-1β secretion via ELISA. Supernatant from cells treated with Nigericin were diluted 1:50 in 1× ELISA/ELISPOT diluent

and those treated with ATP were diluted 1:10 in 1× ELISA/ELISPOT diluent so that the absorbance readings would fall along the sensitivity range of the kit. Once the data was collected, the results were multiplied by the respective dilution factors to account for the dilution. In **Figure 5**, results of the IL-1β ELISA are displayed as fold change with respect to the IL-1β concentration from the supernatants of the WT bone-marrow derived macrophages. Although the results are not significant, the trend observed still supports the results of the previous immunoblotting. This is likely due to the significant variation in IL-1β levels among the various experiments conducted. The TRAF1$^{-/-}$ macrophages indicated a 1.04- and 1.06-fold increase in IL-1β secretion compared to the WT when treated with ATP for 1 and 3 hours, respectively. When treated with nigericin, a 1.2- and 1.3-fold increase in IL-1β secretion was observed in the TRAF1$^{-/-}$ supernatant compared to that from the WT macrophages. These results are consistent with the results of the immunoblotting and suggest that TRAF1 plays a role in controlling the activation of the inflammasome in-vivo, as indicated by both mature IL-1β secretion and caspase-1 processing.

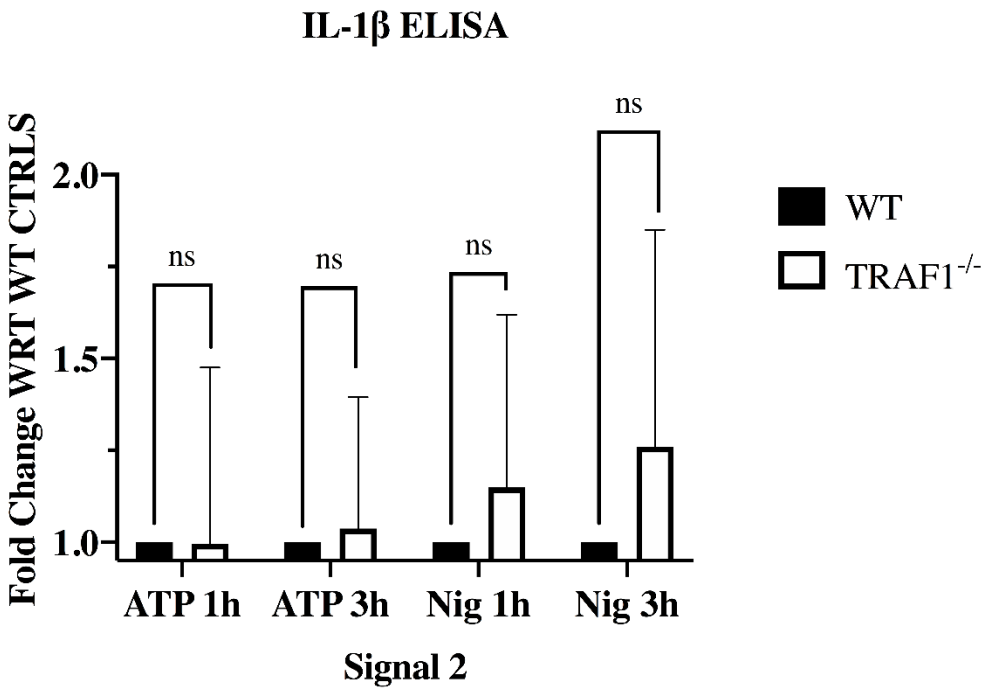

Figure 5. *IL-1β ELISA conducted on supernatant of inflammasome-activate murine bone marrow derived macrophages.* Bone marrow derived macrophages from TRAF1$^{-/-}$ and WT mice were treated with LPS (100 ng/mL) for 3 hours prior to stimulations with ATP (5 mM) and Nigericin (10 µM) for 1 and 3 hours. The culture supernatants were collected, diluted (1:50 for nigericin and 1:10 for ATP) and added to a coated ELISA plate. Fluorescence was measured and used to determine the concentration of secreted IL-1β in each sample. Chart shows fold change in IL-1β secretion with respect to average concentration of the WT samples. Chart includes data from 4 independent experiments. *=p< 0.05, **=p<0.01, ***=p<0.001, ****=p<0.0001 by two-way ANOVA.

4.2 TRAF1 Reduces Innate Immune Cell Recruitment in Peritonitis

4.2.1 Mouse IL-1β ELISA

Figure 6 contains 2 graphs of the IL-1β ELISA results from the supernatant analyzed in two separate MSU-induced peritonitis experiments conducted. In the experiments, mice were injected with 5 mg/mL MSU in PBS -/- and then sacrificed either 4 or 8 hours following the time of the injection. The supernatant was obtained by washing the peritoneum with 3 mL of PBS -/- and then spinning down the sample. The pelleted cells were analyzed via flow cytometry and some of the supernatant was plated on a coated ELISA plate. The results of this analysis were not

significant, but still support the trends described in the immunoblotting and IL-1β ELISA done on the bone marrow derived macrophages. The higher variability and lack of statistical significance observed was due to the samples becoming too being diluted by the PBS -/- from the peritoneal lavage. This resulted in some of the samples falling below the detection limit of the assay. In the 4-hour condition of one experiment, male WT mice averaged a secreted IL-1β concentration of 2.5 pg/mL compared to 13.2 pg/mL for the male TRAF1$^{-/-}$ mice. On average, this is a 5.3-fold increase in IL-1β secretion. For the male mice in the 8-hour condition, the TRAF1$^{-/-}$ mice averaged an IL-1β secretion concentration of 4.5 pg/mL compared to 0.3 pg/mL for the WT mice. This increase in IL-1β secretion is 13.7-fold, on average. When females were in the 4-hour condition, the WT mice averaged a secreted IL-1β concentration of 6.2 pg/mL compared to 0.7 pg/mL for the TRAF1$^{-/-}$ mice. We predict that this observation is especially due to the high variability of the samples, as it does not match the trends reported in any of the other results noted. In the 8-hour condition, female WT mice averaged an IL-1β concentration of 4.8 pg/mL compared to 16.7 pg/mL for the female TRAF1$^{-/-}$ mice. This is an average 3.4-fold increase in IL-1β secretion. These results are also consistent with those assessing inflammasome activation in bone marrow derived macrophages from TRAF1$^{-/-}$ mice. This data indicates a possible trend towards increased IL-1β secretion in TRAF1$^{-/-}$ mice while experiencing an inflammasome-dependent inflammation.

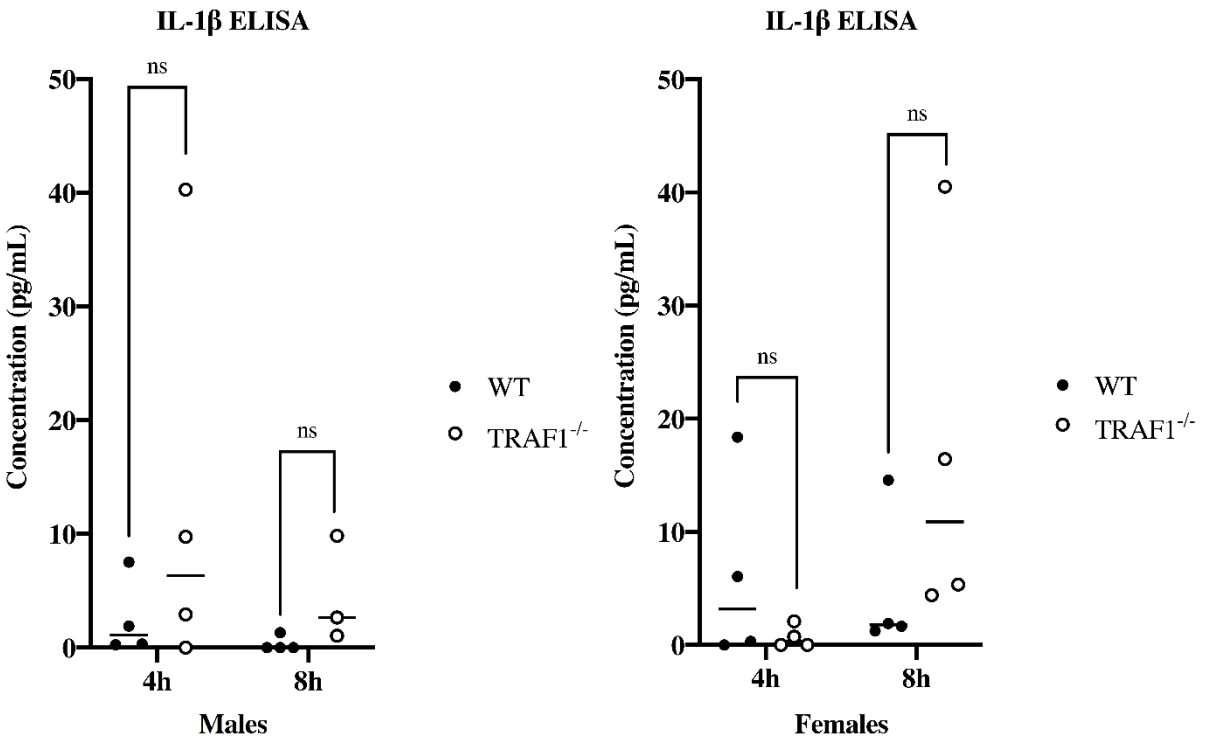

Figure 6. *IL-1β ELISA results from peritoneal supernatant of mice after MSU-induced peritonitis.* After incubation following intraperitoneal injection of MSU, a peritoneal lavage was completed and the extracted PBS -/- was spun down and supernatant was collected to be added to a coated IL-1β plate. Fluorescence was measured and used to determine the concentration of secreted IL-1β in each sample. Chart shows mean of secreted IL-1β concentration for each condition. Each dot represents samples collected from one individual mouse. *=p< 0.05, **=p<0.01, ***=p<0.001, ****=p<0.0001 by two-way ANOVA.

4.2.2 Flow Cytometry

Aside from the supernatant used for IL-1β ELISA, the cells pelleted by centrifuge were resuspended in a prepared antibody staining mix including antibodies for CD45, which was used to identify leukocytes. LY6G and CD11b, to identify neutrophils as well as macrophages and monocytes. F4/80 was also used to identify monocytes, monocyte-derived macrophages, and tissue-resident macrophages. The results of the analysis of the flow cytometry data for male and female mice are displayed in the charts in **Figure 7**, respectively.

For total leukocytes, female WT mice injected with MSU for 4 hours experienced recruitment of about 94,700 leukocytes to the peritoneum. In the same condition, TRAF1$^{-/-}$ mice experienced an average recruitment of about 191,000 leukocytes, which is a 2.0-fold increase compared to the TRAF1$^{-/-}$ mice. The difference between the recruitment of total leukocytes between female TRAF1-/- and WT 4 hours after MSU injection was statistically significant at the $p < 0.05$ level. For 8-hour MSU treatment condition, female TRAF1$^{-/-}$ mice saw the recruitment of an average of 144,000 leukocytes compared to 117,000 leukocytes in the WT mice. This was a 1.2-fold increase in leukocyte recruitment in the female TRAF1$^{-/-}$ mice compared to WT. The difference between the means of these groups was not statistically significant. Male TRAF1$^{-/-}$ mice injected with MSU for 4 hours experienced recruitment of about 106,000 leukocytes to the peritoneum. In the same condition, WT mice experienced an average recruitment of about 125,000 leukocytes, which is a 1.2-fold increase compared to the TRAF1$^{-/-}$ mice. For 8-hour MSU treatment condition, male TRAF1$^{-/-}$ mice saw the recruitment of an average of 191,000 leukocytes compared to 161,000 leukocytes in the WT mice. This was a 1.2-fold increase in leukocyte recruitment in the male TRAF1$^{-/-}$ mice compared to WT. The differences between the means of these groups were not statistically significant.

For neutrophil recruitment, female WT mice experienced an average of 26,200 recruited neutrophils to the peritoneum compared to an average of 78,600 neutrophils recruited for the TRAF1$^{-/-}$ mice in the 4-hour MSU condition. The difference between these groups was significant at the $p < 0.05$ level. This also represents a 3.0-fold increase in neutrophil recruitment. Female WT mice experienced recruitment of an average of 14,000 neutrophils in the 8-hour MSU condition compared to 27,000 in TRAF1$^{-/-}$ mice. This difference was not statistically significant but represents a 1.9-fold increase in neutrophil recruitment for female

TRAF1$^{-/-}$ mice compared to WT. Male WT mice experienced an average of 35,700 recruited neutrophils to the peritoneum compared to an average of 46,700 neutrophils recruited for the TRAF1$^{-/-}$ mice in the 4-hour MSU condition. This represents a 1.3-fold increase in neutrophil recruitment, and the difference between the groups was not statistically significant. Male WT mice experienced recruitment of an average of 25,700 neutrophils in the 8-hour MSU condition compared to 38,400 in TRAF1$^{-/-}$ mice. This difference was not statistically significant but represents a 1.5-fold increase in neutrophil recruitment for male TRAF1$^{-/-}$ mice compared to WT.

Female TRAF1$^{-/-}$ mice were observed to have an average of 18,100 monocytes recruited to the peritoneum in the 4-hour treatment condition, compared to 11,500 for the WT mice. Female TRAF1$^{-/-}$ mice also exhibited recruitment of 16,600 monocytes in the 8-hour treatment condition, compared to 18,100 in the WT mice. These results represented a 1.6-fold increase in monocyte recruitment in TRAF1$^{-/-}$ mice compared to WT in the 4-hour condition and a 1.1-fold increase in monocyte recruitment in WT mice compared to TRAF1$^{-/-}$ in the 4-hour condition. These differences between groups were also not statistically significant here. Male TRAF1$^{-/-}$ mice were observed to have an average of 12,200 monocytes recruited to the peritoneum in the 4-hour treatment condition, compared to 16,400 for the WT mice. Male TRAF1$^{-/-}$ mice also exhibited recruitment of 19,200 monocytes in the 8-hour treatment condition, compared to 18,700 in the WT mice. These results represented a no increase in monocyte recruitment in male TRAF1$^{-/-}$ mice compared to WT in the 8-hour condition and a 1.4-fold increase in monocyte recruitment in male WT mice compared to TRAF1$^{-/-}$ in the 4-hour condition. These differences between groups were not statistically significant here.

Macrophages derived from recruited monocytes were counted at 38,000 for female TRAF1$^{-/-}$ mice and 19,900 for WT mice in the 4-hour MSU treatment condition, on average. This

is a 1.9-fold increase in monocyte-derived macrophages for female TRAF1$^{-/-}$ mice compared to WT. The difference here was not statistically significant. In the 8-hours of MSU condition, an average of 60,800 monocyte-derived macrophages were counted in female TRAF1$^{-/-}$ mice, compared to 51,100 in WT mice. This is a 1.2-fold increase in monocyte-derived macrophage count in the female TRAF1$^{-/-}$ mice compared to WT. An average of 21,700 monocyte-derived macrophages were counted for male TRAF1$^{-/-}$ mice and 33,300 for WT mice in the 4-hour MSU treatment condition. This is a 1.5-fold increase in monocyte-derived macrophages for male WT mice compared to TRAF1$^{-/-}$. The difference here was not statistically significant. In the 8-hours of MSU condition, an average of 73,700 monocyte-derived macrophages were counted in male TRAF1$^{-/-}$ mice, compared to 38,700 in WT mice. This is a 1.9-fold increase in monocyte-derived macrophage count in the TRAF1$^{-/-}$ mice compared to WT. The difference between groups in the 8-hour condition was statistically significant at the $p < 0.05$ level.

Lastly, resident peritoneal macrophages in female WT mice were counted at an average of 4,400 cells in the 4-hour MSU condition. The TRAF1$^{-/-}$ counterparts in the same condition had an average of 2,200 resident macrophages. In this condition, female WT mice had about double the number of resident macrophages compared to the TRAF1$^{-/-}$ mice. At 8 hours, female WT mice had an average of 1,200 resident macrophages, compared to an average of 840 in the TRAF1$^{-/-}$ group. Here, WT mice had about 1.4-times as many resident cells than the TRAF1$^{-/-}$ mice. The differences between the female WT and TRAF1$^{-/-}$ mice for both treatment times were not statistically significant. Male WT mice had an average of 1,100 resident macrophages in the 4-hour MSU condition. The TRAF1$^{-/-}$ counterparts in the same condition had an average of 2,900 resident macrophages. In this condition, male TRAF1$^{-/-}$ mice had about 2.5-times the number of resident macrophages compared to the WT mice. The difference between male TRAF1$^{-/-}$ and WT

mice was significant at the $p < 0.01$ level. At 8 hours, male WT mice had an average of 8,600 resident macrophages, compared to an average of 5,400 in the TRAF1$^{-/-}$ group. Here, WT mice had about 1.6-times as many resident cells than the TRAF1$^{-/-}$ mice. The differences between the male WT and TRAF1$^{-/-}$ mice for both treatment times was also not statistically significant. Interestingly, when we compared the data of the male and female mice within the same treatment conditions, we noticed that male mice had more peritoneal macrophages in three of the four groups compared to female. In WT mice treated with MSU for 4 hours, we observed that female mice had about 3.8 times more resident macrophages on average. However, males had 1.3, 7.1, and 6.4 times more peritoneal macrophages in the TRAF1$^{-/-}$ 4-hour, WT 8-hour, and TRAF1$^{-/-}$ 8-hour groups. The only one of these differences that was statistically significant was that comparing WT male and female mice in the 8-hour condition, which was significant at the $p < 0.01$ level.

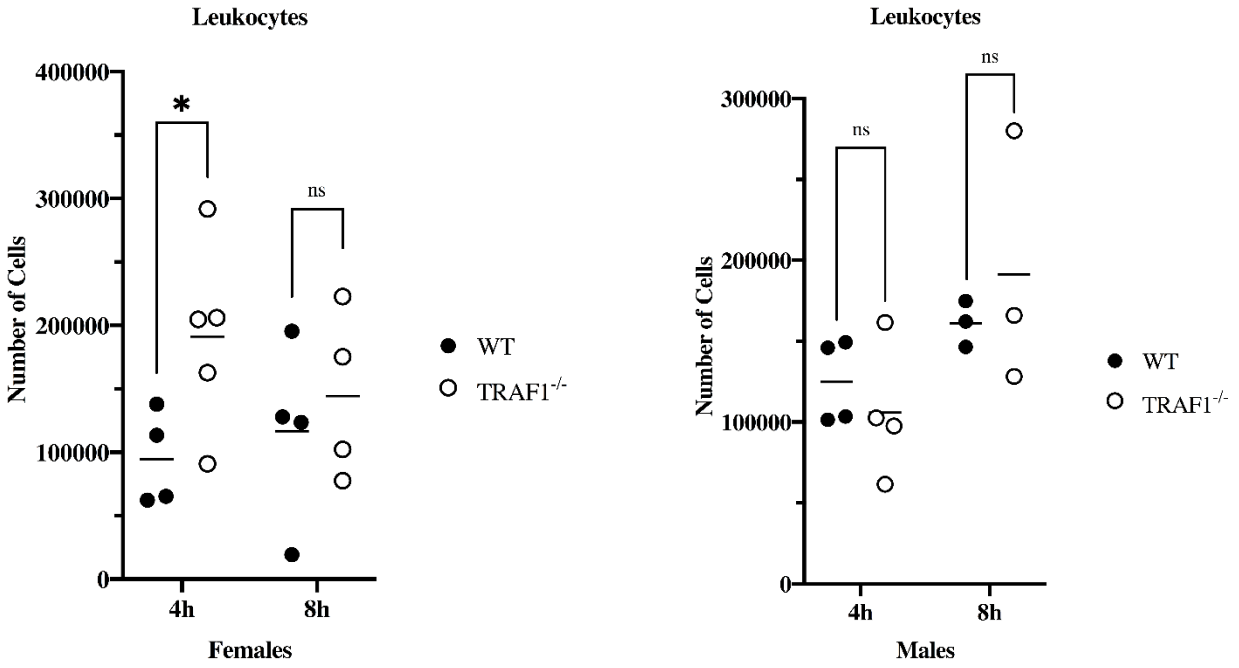

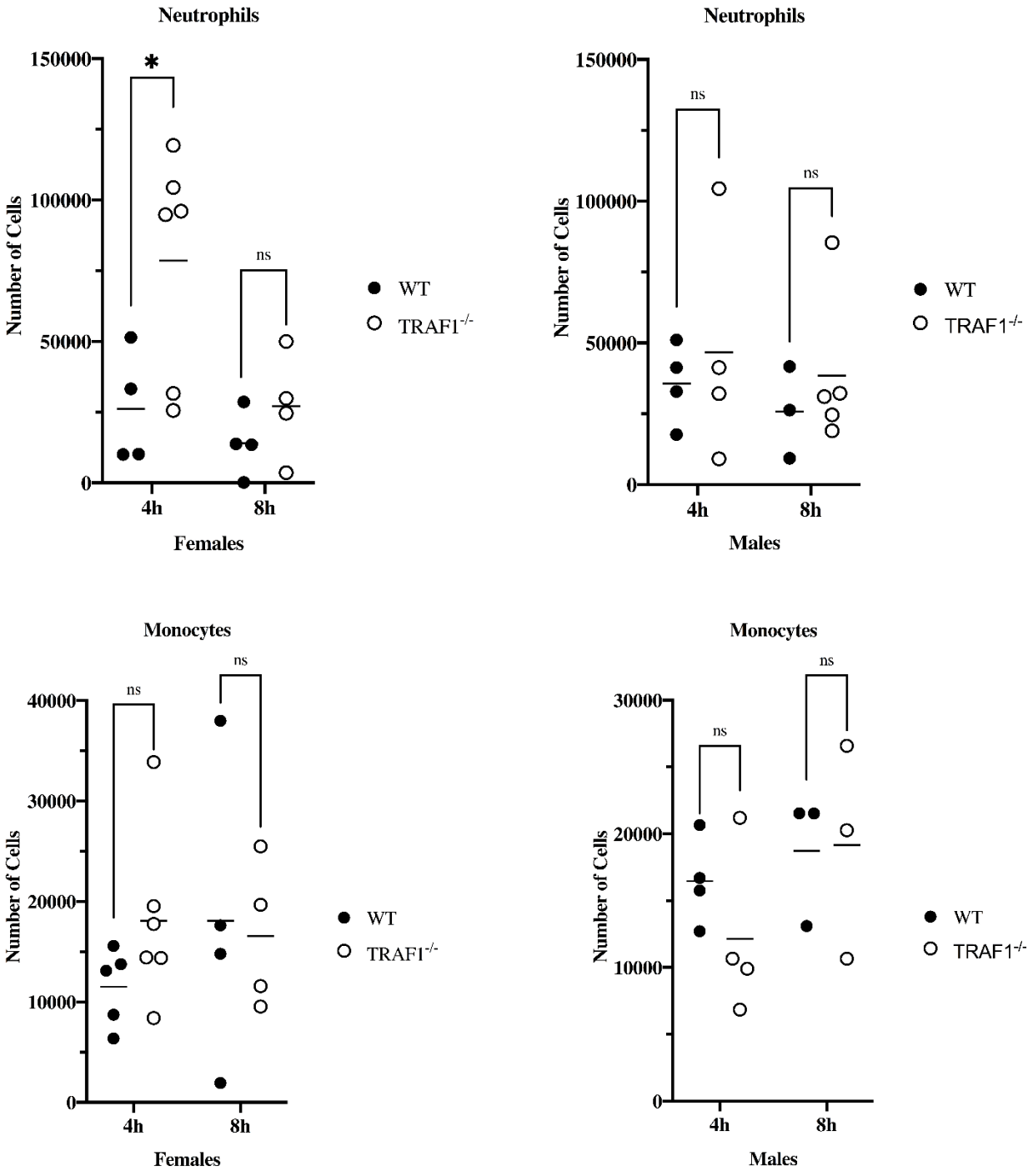
Neutrophils
150000
100000
50000
0
Number of Cells
*
ns
4h
8h
Females
WT
TRAF1-/-
Neutrophils
150000
100000
50000
0
Number of Cells
ns
ns
4h
8h
Males
WT
TRAF1-/-
Monocytes
40000
30000
20000
10000
0
Number of Cells
ns
ns
4h
8h
Females
WT
TRAF1-/-
Monocytes
30000
20000
10000
0
Number of Cells
ns
ns
4h
8h
Males
WT
TRAF1-/-

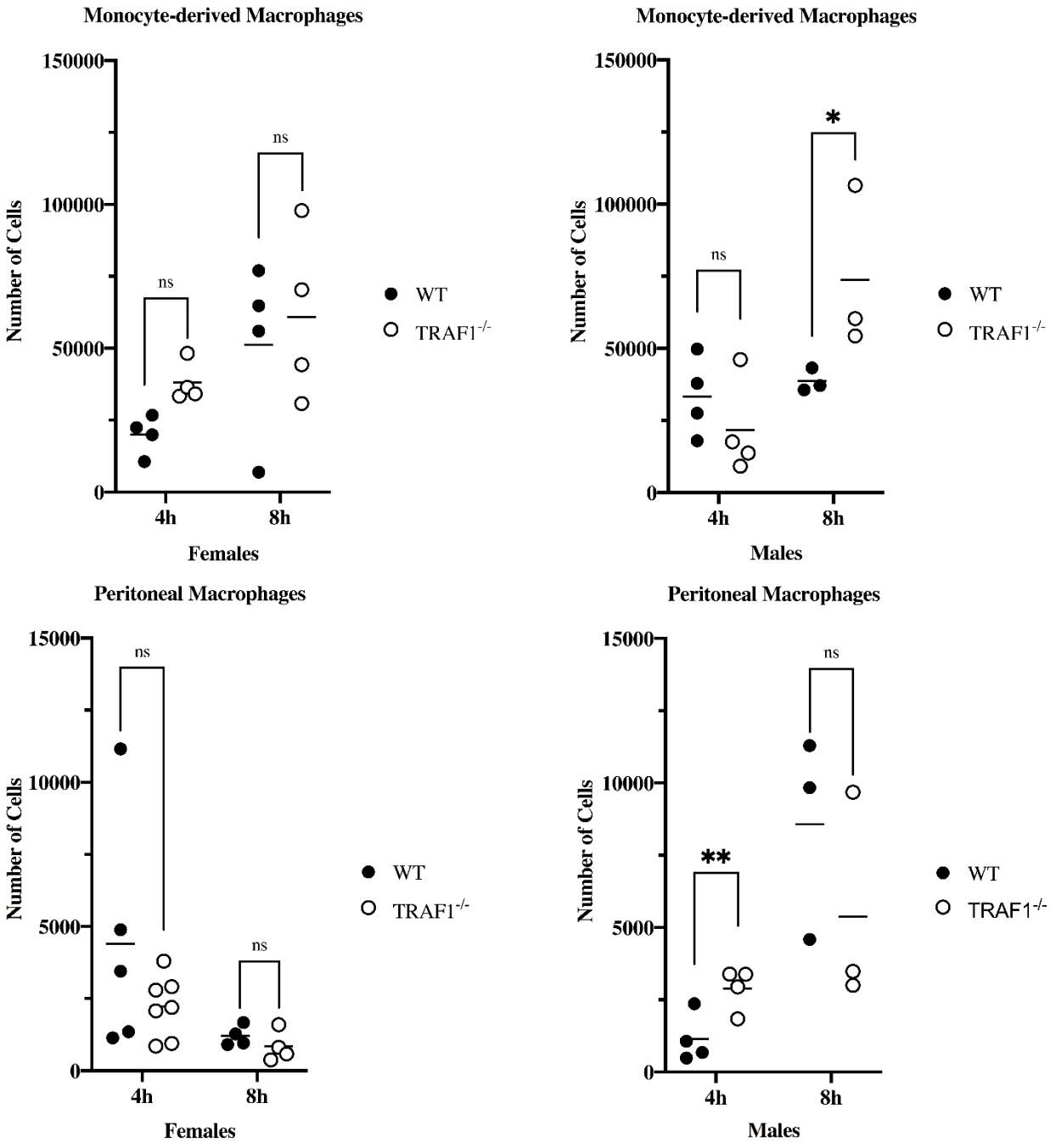

Figure 7. *Flow cytometry analysis of immune cells in male and female mice after MSU-induced peritonitis.* After incubation following intraperitoneal injection of MSU, a peritoneal lavage was completed and the extracted PBS -/- was spun down. Supernatant was removed and the remaining cells underwent red blood cell lysis, Fc blocking and antibody staining to assess recruitment of innate immune cells to the peritoneum. Cells were stained with CD45, LY6G, CD11b, and F4/80 antibodies to identify leukocytes, neutrophils, monocytes, and macrophages. Each dot represents samples collected from an individual mouse. *=p< 0.05, **=p<0.01, ***=p<0.001, ****=p<0.0001 by two-way ANOVA.

4.3 TRAF1 Reduces Markers of Inflammatory Arthritis

4.3.1 TRAF1 Reduces Joint Swelling in Arthritic Mouse Knees

To determine the extent of inflammation in knees injected with MSU and MSU + PA, an electronic caliper was used to measure the joint thickness of each mouse before, immediately after, as well as 2 and 4 hours following intraarticular injections. A summary of the measurements taken is presented in **Figure 8**. In either treatment condition, no mice showed any changes in join thickness immediately following the intraarticular injection. 2 hours following injections, WT mice injected in the MSU condition had an average increase of 0.35 mm in joint thickness. TRAF1$^{-/-}$ mice in the same condition displayed an average increase of 0.57 mm in joint thickness. Although more swelling occurred in the TRAF1$^{-/-}$ mice, the results were not statistically significant. In the MSU + PA condition, WT mice, on average, experienced a 0.21 mm increase in joint thickness 2 hours following injection. TRAF1-/- mice had their joint thickness increase an average of 0.24 mm; the difference between these results was also not significant. 4 hours following injection with of MSU only, the joint thickness of WT mice increased 0.85 mm, on average. TRAF1$^{-/-}$ mice experienced an average increase of 1.39 mm in joint thickness. This difference between the WT and TRAF1$^{-/-}$ mice was significant at the $p < 0.01$ level. 4 hours following injection with MSU + PA, WT mice joints increased in thickness an average of 0.57 mm. TRAF1$^{-/-}$ mice displayed an average increase of 0.90 mm in joint thickness following injections in the MSU + PA condition. The difference between joint thickness in this condition between groups was significant at the $p < 0.0001$ level. Both groups of mice injected with PBS -/- showed no significant increases in joint thickness at any timepoint.

Representative images of injected knee joints 4 hours following intraarticular injections are shown in **Figure 9**. **Figure 9A** shows a knee joint injected with PBS -/-; the thickness of this

joint did not change following injection (remained at thickness of 3.12 mm, shown in **Figure 9A**) and is indicative of a knee prior to any injections. **Figure 9B** is an image of a knee joint of a WT mouse 4 hours after injection with MSU only. Following injection, the joint thickness displayed an increase of 0.75 mm (3.25 mm pre-injection to 4.0 mm shown in the image). The knee joint is clearly swollen and lager than the PBS-injected counterpart. **Figure 9C** shows a knee joint of a $TRAF1^{-/-}$ mouse 4 hours after injection with MSU only. Following injection, this knee showed a 1.91 mm increase in joint thickness (3.4 mm pre-injection to 5.31 mm shown in the image). In **Figure 9C**, there is more swelling, and inflammation compared to both **9A** and **9B**. Also, in data not shown here, the postdoctoral fellow did hematoxylin and eosin staining on the joints and found significantly increased inflammatory cell infiltration in the $TRAF1^{-/-}$ mice.

Altogether, the absence of TRAF1 in this model of inflammatory arthritis is also consistent with previous findings in this thesis. In this physiologically relevant model of RA, joint swelling is significantly increased in $TRAF1^{-/-}$ mice, which supports the hypothesis and previously reported trends indicating TRAF1's role in controlling inflammation.

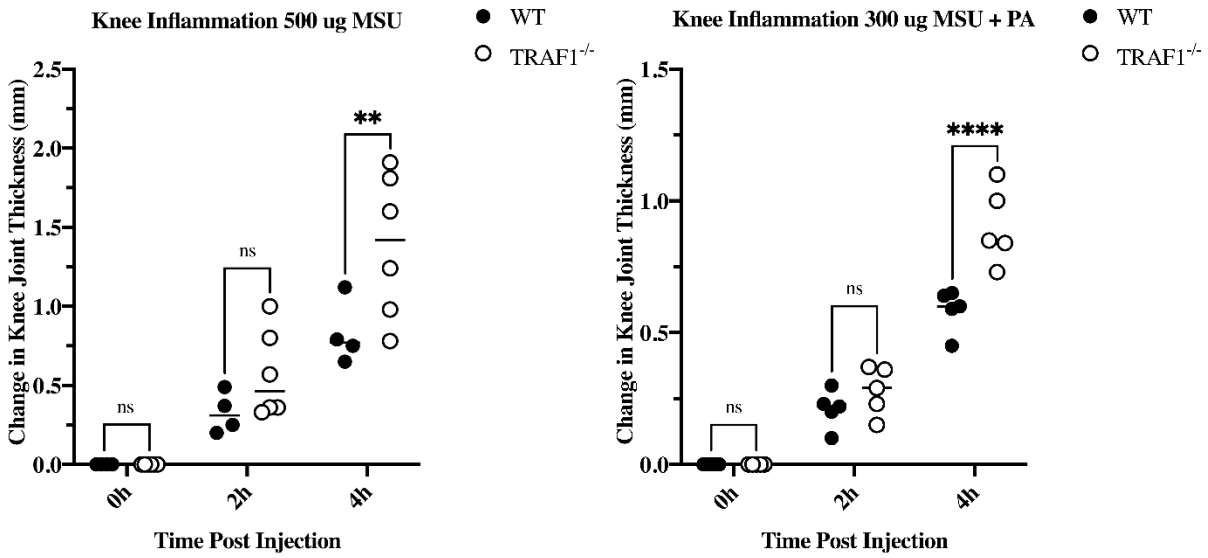

Figure 8. *Change in joint thickness after intraarticular injections of MSU and MSU + PA.* Mouse hind leg knee joint thickness measurements presented as change from their pre-injected thickness. Measurements were made with an electronic caliper prior to, immediately following and 2 and 4 hours post intraarticular injections with either 500 µg of MSU or 300 µg MSU + 0.5 mM PA. Each dot represents a single joint. *=p< 0.05, **=p<0.01, ***=p<0.001, ****=p<0.0001 by two-way ANOVA.

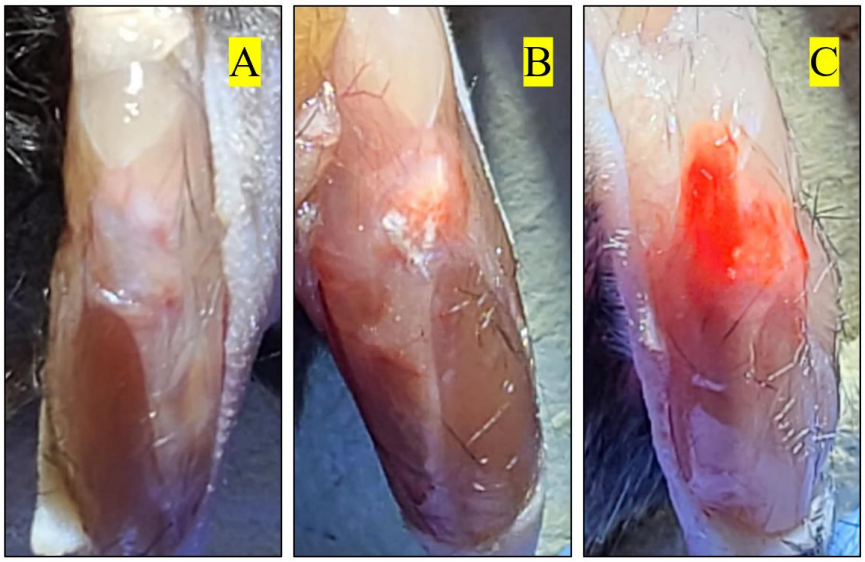

Figure 9. *Images of hind knee joints 4 hours post intraarticular injections with PBS and MSU in WT and TRAF1$^{-/-}$ mice.* Representative images of mouse hind leg knee joints 4 hours following intraarticular injection with PBS -/- in a TRAF1$^{-/-}$ mouse (A), 500 µg MSU in a WT mouse (B), and 500 µg MSU in a TRAF1$^{-/-}$ mouse (C). (A) remained at a thickness of 3.12 mm immediately following, 2 and 4 hours post injection with PBS -/-. (B) had an initial thickness of 3.25 mm, grew

to 3.55 mm 2 hours post injection and was 4.0 mm thick 4 hours post injection (total change of 0.75 mm). (C) had an initial thickness of 3.4 mm, grew to 4.2 mm 2 hours after injection, and 5.31 mm 4 hours post injection (total change of 1.91 mm).

4.3.2 TRAF1 Inhibits Expression of Pro-inflammatory Genes

Once intra-articular injections stimulating crystal-induced arthritis were completed, the synovia of the mice were dissected by a post-doctoral fellow from our lab with significant expertise on the procedure. Following the dissection, each synovium was cut in half. The half of each synovium used for analysis of gene expression was homogenized, and RNA was extracted. Then, cDNA was made from the RNA via reverse transcription and combined with various primers to assess the expression of various genes integral to inflammation and the activation of the NLRP3 inflammasome via real-time PCR. The genes analyzed were *RPLP0, MCP5, IL-1β, IL-6, CXCL10, TNFα, IL-18, Caspase-1, NLRP3, PYCARD (ASC),* and *AIM2*. Once complete, the Cq values were normalized to the expression of the housekeeping gene, RPLP0. **Figure 10** contains the results of the analysis of gene expression and displays them as mean fold change observed in the TRAF1$^{-/-}$ and WT mice in each treatment condition with respect to the mean of the PBS controls.

The gene expression of pro-inflammatory cytokines IL-6 and TNFα, which are secreted in their active form downstream of TLR activation of NF-κB, was significantly higher in TRAF1$^{-/-}$ mice compared to WT controls in all but the MSU + PA condition for TNFα. TRAF1$^{-/-}$ mice exhibited a 33.7-fold increase in expression of *IL-6* compared to a 9.4-fold increase in WT mice in the MSU condition. The difference between the two were significant with a p-value less than 0.01. In the MSU + PA condition, *IL-6* expression increased 32.9-fold for TRAF1$^{-/-}$ mice compared to a 9.3-fold increase for WT. The difference between these two was significant with a p value less than 0.05. Expression of *TNFα* increased 14.3-fold in TRAF1$^{-/-}$ compared to a 4.9-

fold increase in WT mice and was significant at the $p < 0.001$ level in the MSU condition. There did not seem to be a difference between TRAF1$^{-/-}$ and WT mice in the MSU + PA condition for *TNFα*. The difference in expression of *IL-1β* between TRAF1$^{-/-}$ and WT mice was significant with a p-value of less than 0.05 in both the MSU and MSU + PA conditions. TRAF1-/- mice experienced a 24.2- and 27.0-fold increase in *IL-1β* expression in the MSU and MSU + PA conditions, respectively. WT mice only showed a 5.9- and 8.0-fold increase in *IL-1β* expression in the MSU and MSU + PA conditions, respectively. The enhanced expression of the genes responsible for producing these pro-inflammatory cytokines also signifies the role TRAF1 plays in controlling crystal-induced inflammation.

The difference in the expression of NLRP3 inflammasome components *NLRP3, PYCARD (ASC),* and *Caspase-1* was not significantly different in any condition except for one. *NLRP3* expression in the TRAF1$^{-/-}$ mice increased 7.8-fold in the MSU condition compared to 3.8-fold in WT mice. This was significant at the $p < 0.05$ level. The expression of *AIM2* and *IL-18* was also not significantly different in any conditions between the treatments examined. The increased expression of *NLRP3* also support the hypothesis of TRAF1 controlling inflammation in inflammatory disease.

Interestingly, the expression of *MCP5 and CxCL10* was not significantly different in the MSU condition, but WT mice did display significantly more gene expression in the MSU + PA condition. With MCP5, WT mice experienced a 2.6-fold increase in gene expression compared to no change experienced by the TRAF1$^{-/-}$ mice. WT mice experienced a 9-fold increase in expression of *CxCL10* compared to a 2.5-fold increase in TRAF1$^{-/-}$ mice. In both cases, the greater gene expression observed in the WT mice was significant at the $p < 0.05$ level. MCP5 and CxCL10 are both pro-inflammatory chemokines that have been implicated in the

pathogenesis of RA[72]. In the case of the expression of *MCP5 and CxCL10*, TRAF1 seems to play a role in downregulating these genes.

The gene expression of the Ca^{2+} receptors was also significantly different between $TRAF1^{-/-}$ and WT mice at the 0.01 level for S100A8 and 0.05 level for S100A9 for both the MSU and MSU + PA conditions. *S100A8* expression in the MSU condition was 21.1-fold and 24.1-fold in the MSU + PA condition for $TRAF1^{-/-}$ mice. For WT mice, expression of *S100A8* was 2.7- and 3.8-fold in the MSU and MSU + PA conditions, respectively. $TRAF1^{-/-}$ mice also exhibited a 44.7- and 57.7-fold increase in expression of *S100A9* in the MSU and MSU + PA conditions, respectively. For WT mice, *S100A9* expression increased 2.9-fold in the MSU condition and 5.0-fold in the MSU + PA condition. Also consistent with out hypothesis, in the absence of TRAF1, the expression of *S100A8 and S100A9*, which are enhancers of MSU-induced NLRP3 inflammasome activation, is upregulated.

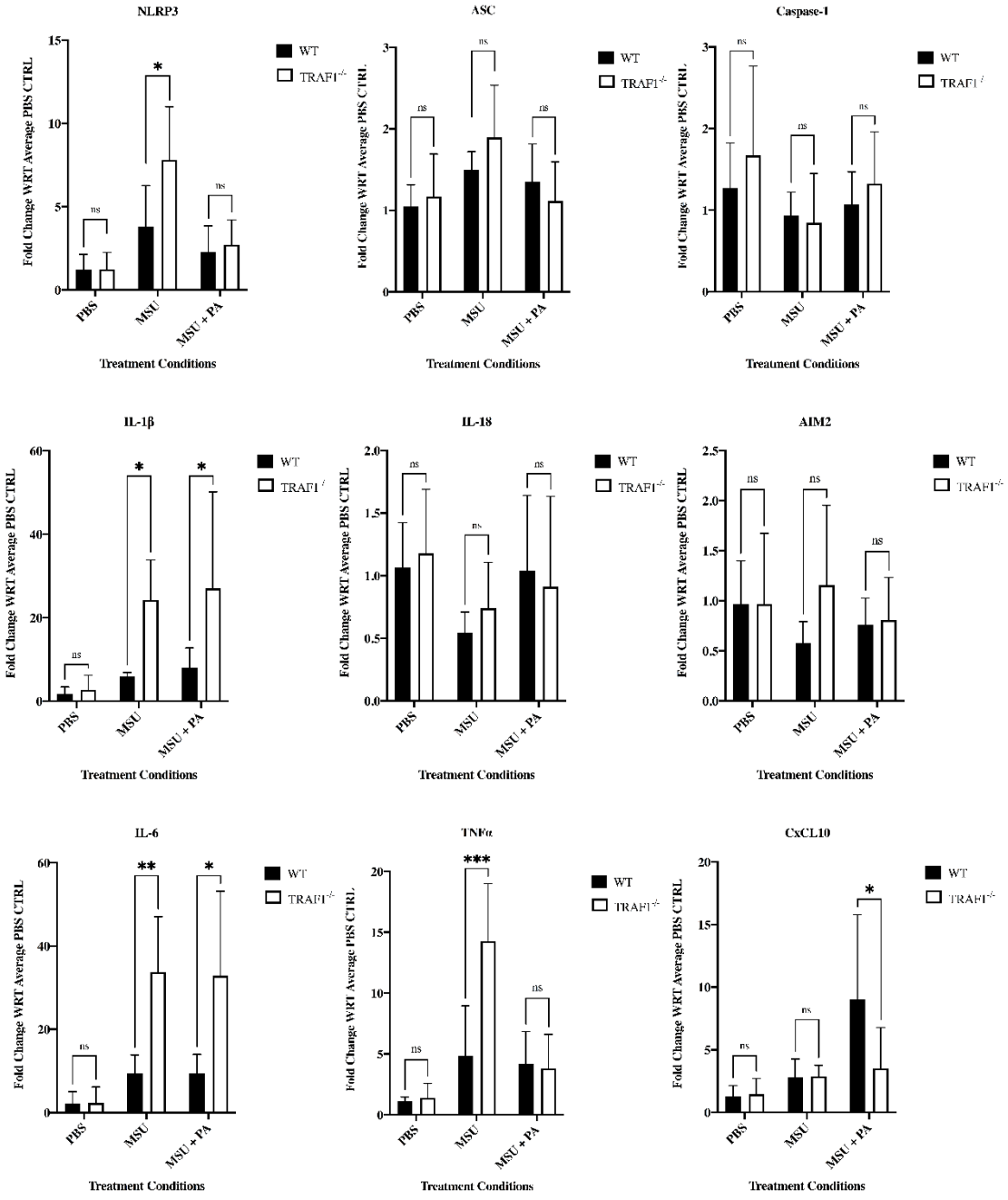
NLRP3
ASC
Caspase-1
IL-1β
IL-18
AIM2
IL-6
TNFα
CxCL10
WT
TRAF1-/-
Fold Change WRT Average PBS CTRL
Treatment Conditions
PBS
MSU
MSU + PA
ns
*
**
***

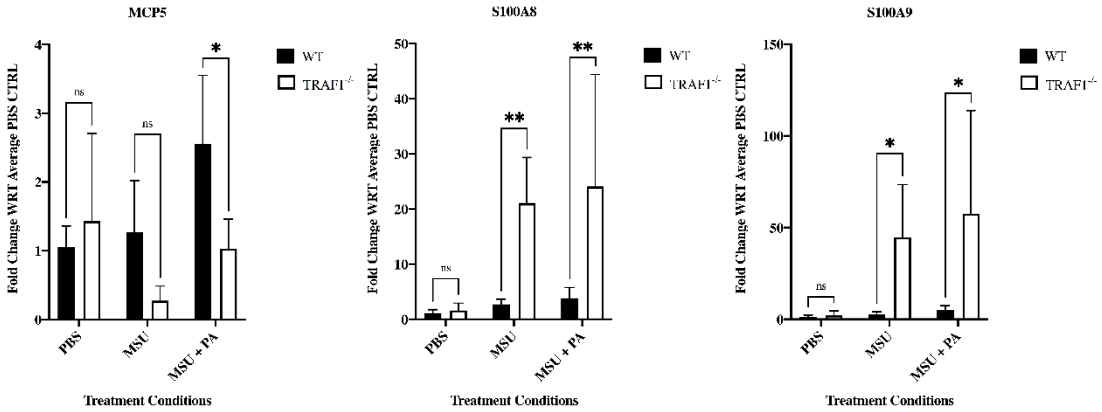

Figure 10. *Real-time PCR results indicating gene expression of markers of NLRP3 inflammasome activation following intra-articular PBS, MSU and MSU + PA injections.* cDNA created from RNA extracted from synovia of mice treated with PBS, 500 mg MSU or 300 mg MSU and PA was analyzed for expression of *IL-6, TNFα, IL-1β, IL-18 NLRP3, PYCARD (ASC), Caspase 1, AIM2, MCP5, CxCL10, S100A8 and S100A9.* Bars indicate fold change of Cq (normalized to housekeeping gene, RPLP0) with respect to the mean fold change of PBS controls. Values are means and standard deviations. Each condition contained at least 4 mice. *=p< 0.05, **=p<0.01, ***=p<0.001 by two-way ANOVA.

4.4 Successful Detection of TRAF1 V203A Mutation

TRAF1 plays a multi-facetted role in regulating NLRP3 inflammasome activation by promoting both pro- (via interaction with cIAP2 downstream of TNFR) and anti- (via interaction with LUBAC downstream of TLR) inflammatory pathways. Previous work from our lab has identified the site of interaction between TRAF1/LUBAC (S283) and TRAF1/cIAP2 (V203). Using these identified interaction sites, we are developing a model that will assess the role of TRAF1 in each pathway individually by introducing single mutations of TRAF1 V203 to V203A, and S283 to S283A in the THP-1 cell line. Thus far, we have been able to utilize CRISPR/Cas9 to produce HDR mediated knock-in of the V203A mutation in THP-1 cells.

Following this knock-in, the bulk-edited population of THP-1 V203A cells were sorted into single-cell colonies and allowed to expand. Once expanded, cells from each of the expanded single-cell colonies had their DNA extracted and target site of the HDR amplified using PCR.

The Guide-It Knock-in Screening Kit was then used to perform an enzymatic assay that recognizes the single interrogated base and triggers fluorescence that is detected by the real-time PCR. Green fluorescence indicated homozygous presence of our SNP of interest (V203A), red fluorescence indicated homozygous presence of the WT allele, and a combination of red and green fluorescence indicated that the genotype was heterozygous. No fluorescence meant that neither the SNP of interest nor WT allele were present in the amplified target site. **Figure 11** outlines the results of the screening of our single-clone colonies. Of the 110 different colonies screened, 5 (indicated by 10 blue squares as each sample was analyzed in duplicate) were identified to express green fluorescence only, indicating that the corresponding cells potentially contained the successful homozygous TRAF1 V203A knock-in.

Following the identification of these 5 TRAF1 V203A knock-in clones, the remaining amplified PCR product obtained from earlier steps in the screening process was combined with primers for the target site of simplification were sent for DNA sequencing. The results of the sequencing are in **Figure 12**, which shows that of the 5 populations of expanded clones analyzed, 3 contained the homozygous TRAF1 V203A knock-in without any additional errors or substitutions, as was the case with the remaining 2 clones. The chromographs in **Figure 12** indicate the single point mutation of a thymine to cytosine in the 3 clones, which led to the substitution of Valine 203 with Alanine. According to in-vitro work done by our lab previously, this substitution fails to interact with cIAP2 while maintaining complete interaction with HOIL-1 subunit of LUBAC.

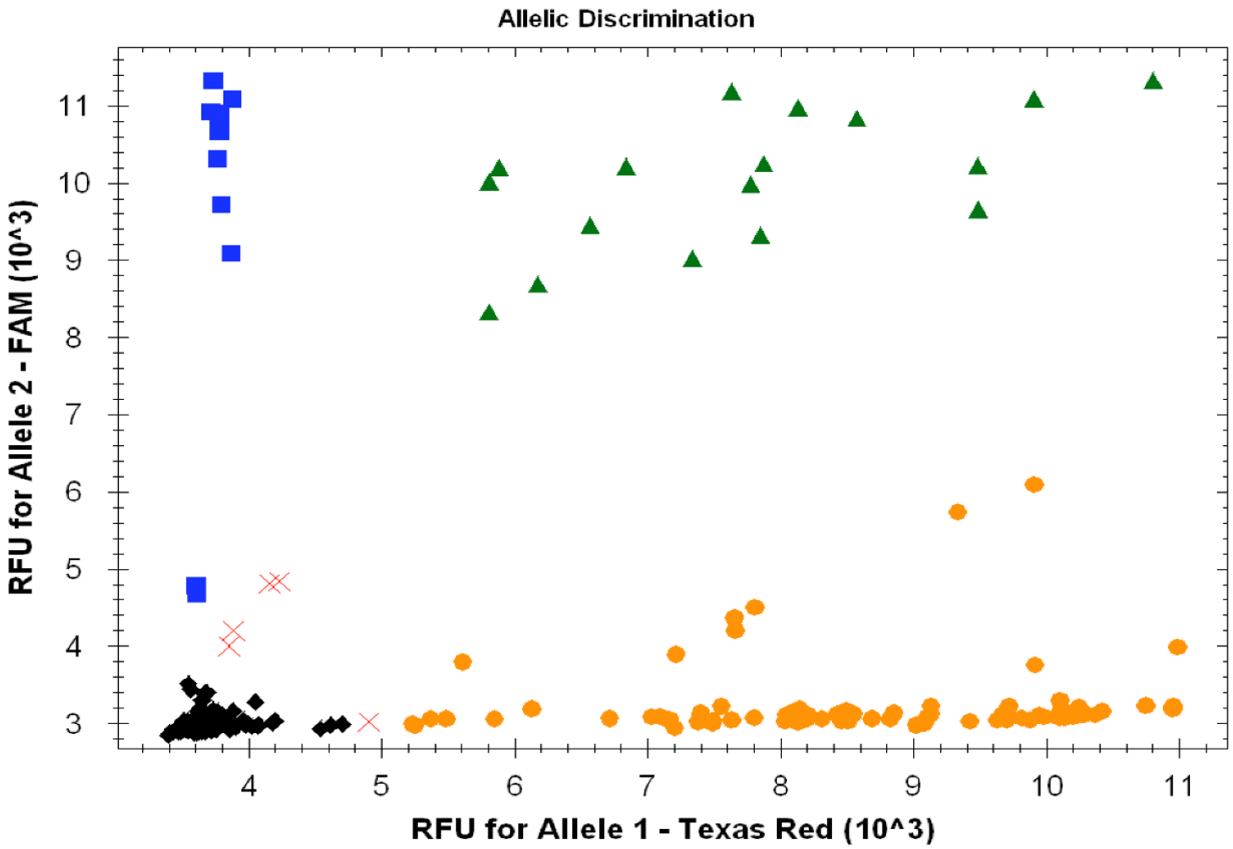

Figure 11. *Allelic discrimination of CRISPR/Cas9 HDR-mediated knock-in of TRAF1 V203A mutation.* Allelic discrimination was used to detect single base pair difference of target sequencies amplified from target sites of DNA extracted from THP-1 cells that underwent CRISPR/Cas9 HDR mediated knock-in of the V203A mutation. Blue squares indicate homozygous V203A mutation, orange circles are homozygous WT genotype, green triangles are the heterozygous genotype. Black diamonds and red crosses did not register in any of the other categories. The cells that corresponded with the targets assessed as homozygous knock-ins were sent for additional sequencing. RFU – Relative fluorescence units.

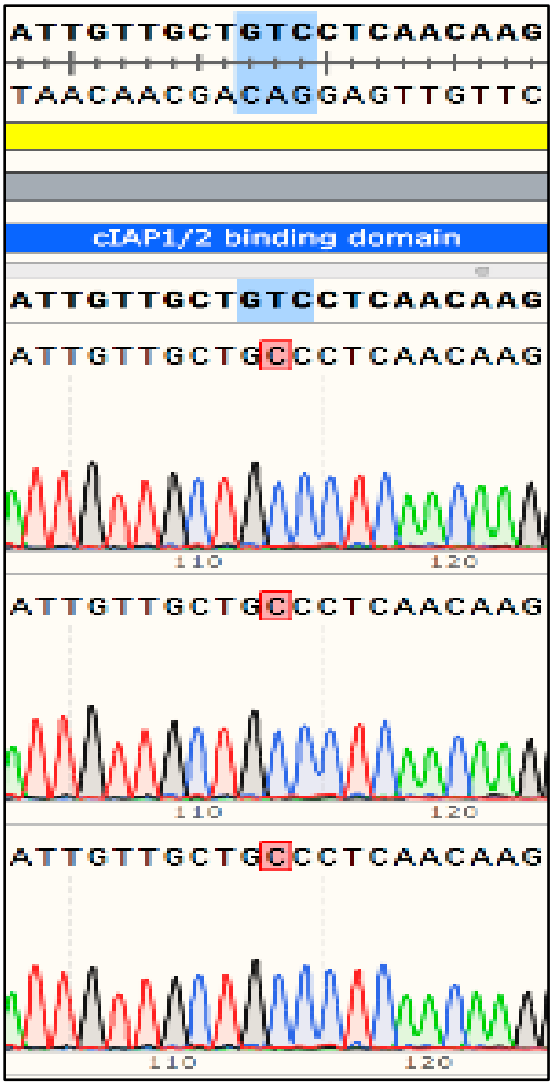

Figure 12. *Sequencing chromatographs for TRAF1 mutant V203A KI in THP-1 cells.* The genomic DNA of clones selected from screening were extracted and purified, followed by PCR amplification of the target site and sequencing. 3 sequencing chromographs for edited allele of TRAF1 gene are shown. Blue peaks denoted C bases. WT sequence is also presented at the top of the figure with region coding for the target amino acid, (Valine 203) highlighted in blue. Chromographs show successful point mutation of Valine 203 into Alanine by substituting thymine base with cytosine.

4.5 TRAF1 V203A Mutation Prevents Inflammasome Activation

4.5.1 Inflammasome Activation is Inhibited in TRAF1 V203A Cells

WT THP-1 and TRAF1 V203A cells were plated and PMA differentiated overnight. Following 3 hours of priming with LPS, cells were treated with either ATP or nigericin for 1 or 3 hours to initiate signal 2 and full NLRP3 inflammasome activation. One sample of each of the TRAF1 V203A and WT cells was left untreated, and one was treated with LPS alone. Once treatments concluded, the proteins present in the supernatant of the cells were precipitated and the expression of IL-1β and caspase-1 were quantified via western blot. These were analyzed because the mature forms of these two proteins are secreted downstream of NLRP3 inflammasome activation. **Figure 13** indicates the results of the protein quantification.

Figure 13 shows the immunoblotting for caspase-1 from the precipitated proteins. Based on the thickness of the bands, which are indicative of protein expression, the WT THP-1 cells express more processing of the 45 kDa pro-caspase-1 (inactive zymogen) into the biologically active 33 kDa caspase-1 in all of conditions fully activating the NLRP3 inflammasome. The blot indicated similar production of the precursor pro-caspase-1 in all treated conditions across both the WT THP-1 and THP1 V203A cells. The blot also indicated more production of the precursor pro-IL-1β in all treated conditions from the WT THP-1 cells compared to the THP1 V203A cells. **Figure 13** also shows the immunoblotting of IL-1β from the precipitated proteins. Based on the thickness of the bands, which are indicative of protein expression, the WT THP-1 cells express more precursor 37 kDa pro-IL-1β, and biologically active 17 kDa IL-1β in all of conditions fully activating the NLRP3 inflammasome. In all blots, protein expression induced by nigericin was much greater than that induced by ATP.

These experiments were conducted with two of the three cell lines from expanded single-cell clones that we identified to contain the successful TRAF1 V203A mutation. The results were consistent across both sets of clones analyzed, and **Figure 13** is representative of the five independent experiments conducted under these conditions.

These results intriguingly indicate that the V203A mutation of TRAF1 in THP-1 cells downregulate the activation of the NLRP3 inflammasome as noted by a decrease in caspase-1 and IL-1β processing.

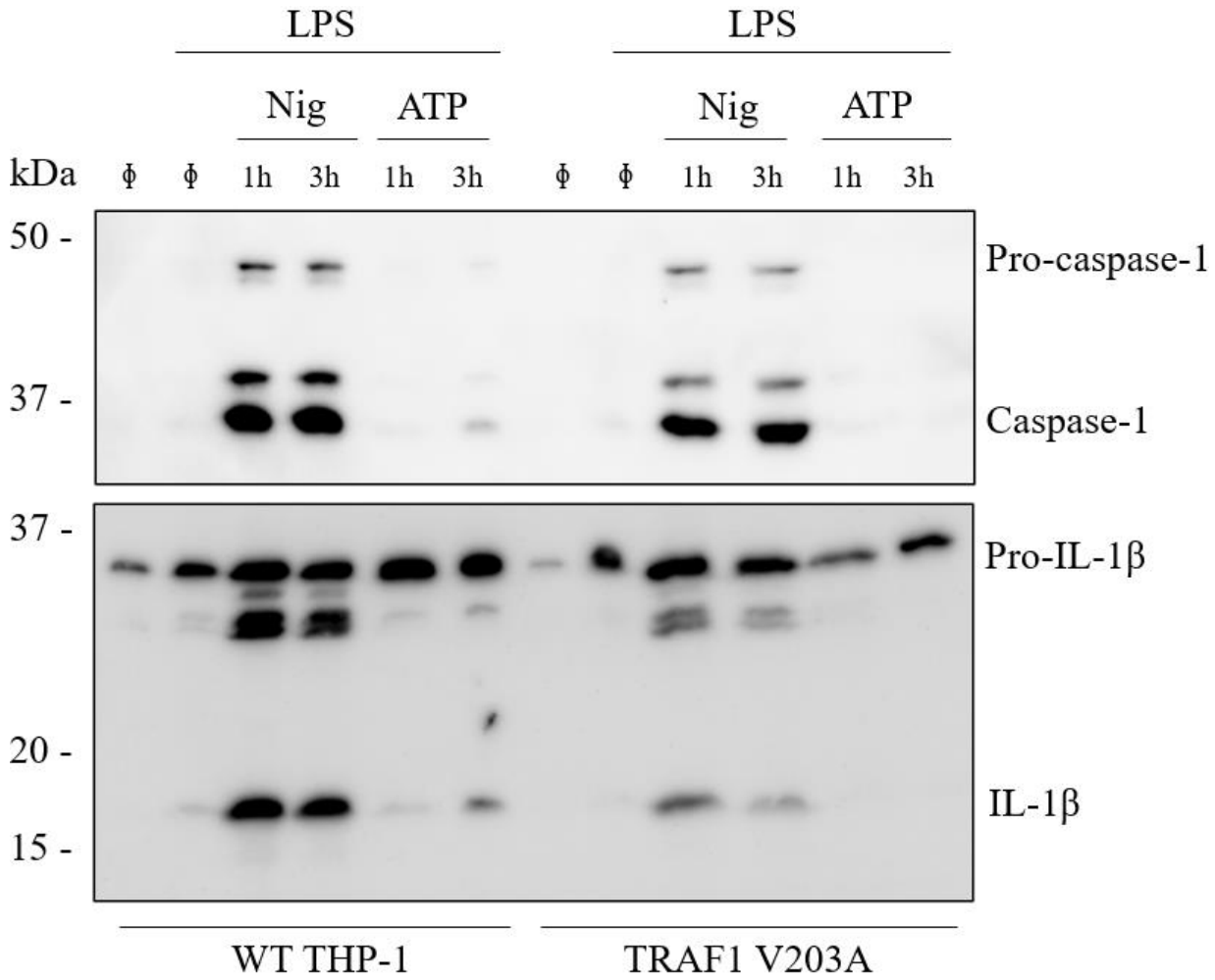

Figure 13. *Caspase-1 and IL-1β processing in WT and TRAF1 V203A KI THP-1 cells*. THP-1 cells were treated with LPS (100 ng/mL) for 3 hours prior to stimulations with ATP (5 mM) and Nigericin (10 μM) for 1 and 3 hours. The culture supernatants were collected, the proteins in the

supernatant were precipitated using 100% TCA and immunoblotted for expression of cleaved and uncleaved caspase-1, as well as cleaved and uncleaved IL-1β. The data shown are representative of five independent experiments with two of the identified clones containing the successful TRAF1 V203A mutation.

4.5.2 NF-κB Activation is Unaffected by TRAF1 V203A Mutation

To better understand the specific mechanism in which inflammasome activation is disrupted by the TRAF1 V203A mutation, WT THP-1 and TRAF1 V203A cells were treated with only LPS for 15 and 30 minutes, as well as 1, 3 and 6 hours to examine the extent of NF-κB activation and production of components required for inflammasome formation following signal 1. Once treatments were completed, cells were collected and lysed. After the amount of protein in each sample was quantified using Bradford reagent, samples were analyzed via western blot.

Figure 14 shows the results of those experiments. As was the case with the experiments assessing inflammasome activation, these experiments were conducted with two of the three cell lines from expanded single-cell clones that we identified to contain the successful TRAF1 V203A mutation. The results were consistent across both sets of clones analyzed, and **Figure 14** is representative of the five independent experiments conducted under these conditions.

Figure 14 shows the expression of 40 kDa phospho-IκBα (p-IκBα). The phosphorylation of IκBα occurs upstream of and is a marker of NF-κB activation. Across all treatments, protein expression in both the WT THP-1 and TRAF1 V203A cells is similar; p- IκBα protein expression shows no expression in the absence of treatment with LPS. When treated with LPS for 15 minutes, protein expression is evident in both cell lines. Protein expression increases slightly at 30 minutes of LPS stimulation and then significantly increases at 1 hour of stimulation. At 3 hours, expression of p-IκBα decreases again and at 6 hours, expression increases slightly once more.

Also, in **Figure 14** is the expression of 39 kDa IκBα. Shortly after phosphorylation of IκBα, it is degraded and allows NF-κB to translocate from the cytoplasm to the nucleus to promote transcription. Therefore, degradation, or absence of IκBα is also a marker of NF-κB activation. In **Figure 14**, it is evident that both the WT THP-1 and TRAF1 V203A cells show similar trends in IκBα degradation. Without stimulation, IκBα expression is clearly present, but once stimulation with LPS begins for 15 minutes, IκBα expression significantly decreases. This degradation occurs even more so at 30 minutes and protein expression only slightly increases into the 1-hour condition. At 3 and 6 hours of stimulation, the response to LPS has subsided and IκBα expression is restored.

Figure 14 also shows the expression of 37 kDa pro-IL-1β, which is a product of transcription promoted by NF-κB. Production of pro-IL-1β does not occur in the conditions that are 1 hour or less, but pro-IL-1β expression can be seen in the 3- and 6-hour conditions. Interestingly, there is less expression of pro-IL-1β in the TRAF1 V203A cells compared to the WT THP-1 cells in both the 3- and 6-hour conditions. The difference between protein expression in the two cell lines is to a greater extent in the 6-hour condition. When combined with the results of the inflammasome activation experiments on the TRAF1 V203A cells, it is evident that the observed decrease in inflammasome activation occurs independently of NF-κB activation or signal 1 of inflammasome activation. However, the decreased expression of pro-IL-1β in TRAF1 V203A cells most likely contributes, in part, to the observed decrease in mature IL-1β release.

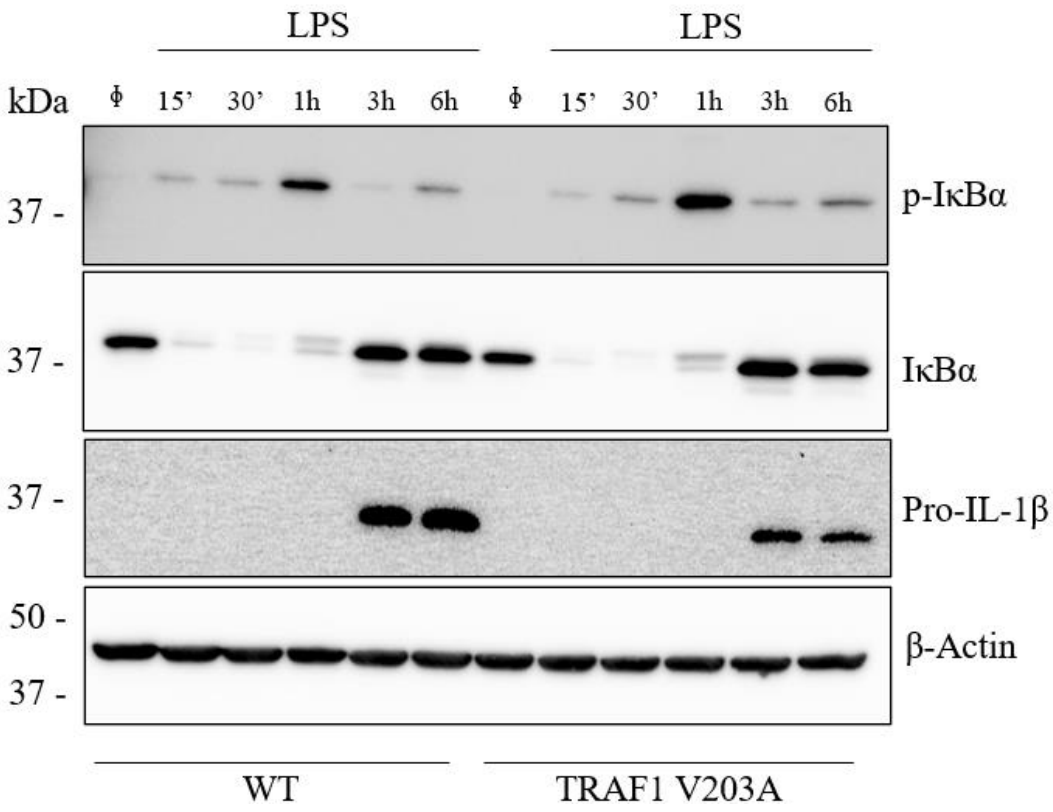

Figure 14. *phospho-IκBα, IκBα and pro-IL-1β expression in WT and TRAF1 V203A KI THP-1 cells.* THP-1 cells were treated with LPS (1 μg/mL) for 15 and 30 minutes, as well as 1, 3 and 6 hours. The cells in suspension were collected, lysed, and immunoblotted for expression of phospho-IκBα, IκBα, pro-IL-1β and β-actin. The data shown are representative of five independent experiments.

Chapter Five: Discussion

Previous in-vitro research has identified that TRAF1 plays a multifaceted role in regulating inflammation by either promoting or inhibiting NF-κB activation downstream of TNFRs and TLRs, respectively. Abdul Sater et al. demonstrated that TRAF1 negatively regulates NF-κB activation by binding directly to components of LUBAC and thereby interfering with the linear ubiquitination of NEMO[57]. Continued research from our lab has also shown that TRAF1 plays an important role in regulating the NLRP3 inflammasome by limiting caspase-1 activation and IL-1β secretion via its inhibition of LUBAC and subsequent NF-κB activation and linear ubiquitination of ASC. The NLRP3 inflammasome acts as a crucial component of innate immunity, and its dysregulation has been implicated in many human auto-inflammatory and auto-immune diseases characterized by excessive IL-1β secretion[34,35]. Also, around 20% of the population have an SNP in their TRAF1 gene associated with RA[65]. Therefore, continuing to understand the underlying mechanism of TRAF1 regulation of NLRP3 activation is critical for developing therapies that allow for specific TRAF1 targeting to improve outcomes of NLRP3 inflammasome-related diseases. To this end, we examined the extent of which TRAF1 regulates NLRP3 inflammasome activation in two in-vivo models of inflammasome-mediated disease.

To begin, we demonstrated that our lab's previous results, which have been conducted in human monocytes, also occur in a murine cell line. These results confirmed that TRAF1 controls NLRP3 inflammasomes in murine bone marrow derived macrophages. Analysis by caspase-1 and IL-1β immunoblotting, and IL-1β ELISA demonstrated that TRAF1$^{-/-}$ mice had greater NLRP3 inflammasome activation compared to WT counterparts. Next, through use of MSU-induced peritonitis and crystal-induced arthritis models, we demonstrated that TRAF1 inhibits NLRP3 inflammasome activation and progression of these inflammasome-dependent diseases in

mice. These conclusions were made based on results indicating reduced innate immune cell recruitment to the peritoneum by flow cytometry, reduced IL-1β secretion by IL-1β ELISA, reduced knee inflammation measured by electronic caliper, and less activation of pro-inflammatory genes in synovia derived from inflammatory-arthritis induced mice. Our findings also showed that when TRAF1's interaction with cIAP2 is interrupted, NLRP3 inflammasome activation, as indicated by caspase-1 and IL-1β immunoblotting, decreases independently of NF-κB activation. Altogether, these findings provide insights that could lead to the development of novel therapies that target TRAF1 to improve outcomes of NLRP3 inflammasome-related diseases such as RA.

First, we needed to confirm that the inhibition of inflammasome regulation mediated by TRAF1 observed in a human cell line also occurred in cells derived from mice. To do this, we stimulated inflammasome activation using LPS as signal 1 and nigericin and ATP as signal 2 in macrophages derived from the bone marrow of $TRAF1^{-/-}$ mice. Immunoblotting for protein expression in the supernatant of these cells as well as IL-1β ELISA were employed to assess the processing and secretion of mature caspase-1 and IL-1β, both of which are released as a result of NLRP3 inflammasome activation. Our results indicate that NLRP3 inflammasome activation is indeed increased in the absence of TRAF1 by way of increased processing and secretion of biologically active caspase-1 and IL-1β. These results are consistent with those conducted by our lab in human monocytes and confirmed the role of TRAF1 in inhibiting inflammasome activation in macrophages derived from mice.

Next, we wanted to assess how TRAF1's control of inflammasome activation impacts the progression of inflammatory diseases. Using a murine MSU-induced peritonitis model, which is a model of inflammasome-dependent inflammation, we assessed the role of TRAF1 in

recruitment of innate immune cells and secretion of IL-1β. Induction of peritonitis was consistent with that described by Spalinger and Scharl in 2018. Most results lacked statistical significance but did indicated trends in increased inflammasome activation by way of increased IL-1β secretion, and subsequent recruitment of total leukocytes, neutrophils and monocytes, as well as differentiation of recruited monocytes into macrophages in the peritoneum in the absence of TRAF1. The recruitment of total leukocytes and neutrophils was significantly greater in female TRAF1$^{-/-}$ mice compared to WT in the 4-hour MSU condition. Male TRAF1$^{-/-}$ mice had significantly more monocyte-derived macrophages and peritoneal macrophages in the 8-hour and 4-hour conditions, respectively.

Interestingly, the significance observed in the female TRAF1$^{-/-}$ mice for leukocyte recruitment disappeared when combined with male mice. Although other results were not significant, the clear trends observed in female mice for the other immune cells assessed also disappeared when combined with results from male mice. It is difficult to speculate on specific sex differences between male and female mice based on this data, but our data do suggest more variation in male mice's response to MSU-induced peritonitis compared to females, and in some cases, less robust differences in immune cell recruitment between WT and TRAF1$^{-/-}$ mice. Our data also indicate a potential trend of a greater macrophage presence in male mice compared to females. Together, these trends provide an intriguing avenue for continuing research on how sex differences may impact TRAF1's control of NLRP3 inflammasome activation. The variation in the results observed here when assessing sex-specific differences in innate immune cell recruitment highlights the diversity and complexity of the mechanisms that may be affected by specific sex differences.

Given the variation in each individual mouse's response to MSU-induced peritonitis, we also believe that increases in immune cell recruitment and IL-1β secretion observed could achieve significant differences with further analysis that increases the number of mice in each treatment condition.

In the assessment of crystal-induced arthritis caused by intraarticular injection of MSU, significant increases in markers of inflammation associated with arthritis were observed in the absence of TRAF1. Injection of MSU or MSU & PA clearly initiated inflammatory arthritis as observed by the increases in joint thickness 2- and 4-hours following injection in both populations of mice. The swelling is described to be due to increased production of pro-inflammatory cytokines like TNFα, IL-6 and IL-1β, and the subsequent recruitment of neutrophils and monocytes to combat the injected MSU crystals[73]. To that end, at 4 hours post injection with both MSU and MSU + PA conditions, TRAF1$^{-/-}$ mice displayed a significant increase in joint thickness compared to WT mice. This significant increase in joint thickness is consistent with previous findings from our lab and in this paper of TRAF1's role in controlling the activation of the NLRP3 inflammasome.

Furthermore, analysis of real-time PCR data confirms that there is increased expression of many pro-inflammatory genes in the synovium extracted from the WT and TRAF1$^{-/-}$ mice injected intraarticularly with MSU and MSU + PA. In the case of the pro-inflammatory cytokine-transcribing genes *TNFα*, *IL-6* and *IL-1β*, TRAF1$^{-/-}$ mice experienced significantly more gene expression compared to that observed in WT mice in either one or both of the MSU and MSU + PA conditions. TRAF1-/- mice also had significantly more expression of *NLRP3* in the MSU condition compared to WT mice. The increased expression of these genes is consistent with our hypothesis of TRAF1 being a key regulator of inflammation via its interaction with LUBAC.

Downstream of TLRs detecting PAMPS in WT mice, TRAF1 inhibits LUBAC's ability to linearly ubiquitinate NEMO and inhibits downstream NF-κB activation, which prevents the promotion of the expression of *TNFα, IL-6, IL-1β* and *NLRP3*[19,20]. Our data shows that when TRAF1 is not expressed, the expression of these genes is subsequently increased and promotes increased inflammation. Although TRAF1$^{-/-}$ mice expression of ASC and caspase-1 was not significant different than that of WT mice, this does not necessarily mean activation of the inflammasome is not increased. We have shown that NLRP3 inflammasome activation does increase in TRAF1$^{-/-}$ mice, rather than this being due to more transcription of its components, this may indicate that the complex is forming and experiencing enhanced activation with the components already present in the cytosol.

Expression of *S100A8 and S100A9* was also significantly increased in TRAF1$^{-/-}$ mice compared to their WT counterparts. MSU has been shown to play a crucial role in the secretion of S100A8/A9, which enhances MSU-induced NLRP3 activation[46]. Our results are consistent with the findings that *S100A8/A9* is elevated in WT and TRAF1$^{-/-}$ mice. Our results also indicate that the absence of TRAF1 promotes the expression of these genes, and further highlighting the importance of TRAF1 as a key modulator of inflammation.

The results of these in-vivo, inflammasome-dependent disease models all suggest that TRAF1 plays an important role in controlling NLRP3 inflammasome activation by way of inhibiting processing and secretion of IL-1β and caspase-1, expression from a variety of pro-inflammatory genes and the subsequent recruitment of innate immune cells to the disease site. These results all add to previous findings by our lab and further implicate TRAF1 as a potential target for treatments for inflammatory diseases as it plays a key role in regulating inflammation via its interaction with LUBAC that inhibits activation of the NLRP3 inflammasome.

Based on the results of screening of the THP-1 cells that had undergone CRISPR/Cas9 HDR-mediated knock-in of the V203A mutation and subsequent DNA sequencing results, we successfully created 3 populations of cells that contain the TRAF1 V203A mutation without any other adverse mutations or deletions. The populations grown from these 3 clones were expanded for experimentation. A member of our lab has begun testing TNFR signalling in one of the populations and their preliminary results indicate that the interaction between TRAF1 and cIAP2 is eliminated in these cells.

Intriguingly, the results of our analysis of the TRAF1 V203A mutant on inflammasome activation were unexpected. Determined by previous research in our lab, the site of the mutation eliminates the interaction between TRAF1 and cIAP2, while maintaining all other interactions with TRAF1. This mutation was created to assess the anti-inflammatory role of TRAF1 in TLR signalling without the pro-inflammatory effects observed as a part of TNFR signalling to better understand the mechanism in which TRAF1 inhibits inflammation. We expected that inflammasome activation would be unaffected since this interaction occurs independently of TLR signalling. However, immunoblotting results from two of the three identified populations containing the TRAF1 V203A mutation indicate that inflammasome activation, via analysis of processing and secretion of caspase-1 and IL-1β, is reduced in these mutant cells. The expression of caspase-1 and IL-1β was assessed by analysis of protein in the supernatant of these cells treated with LPS and either nigericin or ATP at various timepoints. Interestingly, it has been demonstrated that cIAP1/2 interacts with and are important mediators of caspase-1 activation[74]. Results from Labbé's 2011 study determined that cIAP1, cIAP2, and TRAF2 all physically interact with caspase-1 containing complexes and are required for caspase-1 catalysis within the inflammasome[74]. The authors concluded that cIAPs are essential for inflammasome formation

and activation via their role in activating caspase-1 via K63-linked polyubiquitination that is mediated by E3 ligase activity[74]. Previous findings from our lab also indicate that cIAP2 experienced greater and more rapid degradation in the absence of its interaction with TRAF1 in human Burkitt's B-cell lymphoma cells and concluded that TRAF1 preserves the half-life of cIAP2 by protecting it from rapid degradation in immune cells. Using the TRAF1 V203A cells, another lab member has also found that expression of cIAP2 is drastically decreased in these mutant cells. Based on these data, it seems as though the TRAF1 V203A cells no longer interact with or protect cIAP2 from degradation. Moreover, the decrease in cIAP2 levels inhibits caspase-1 activation in the inflammasome, which results in the decreased processing and secretion of both caspase-1 and IL-1β that we observed.

Figure 15 summarizes the multiple roles that TRAF1 plays in regulating NLRP3 inflammasome activation.

We also assessed NF-κB activation by immunoblotting for p-IκBα, IκBα and pro-IL-1β to rule out any aberrant effects on inflammasome priming following signal 1. Our results indicate that phosphorylation and degradation of IκBα is similar between both WT THP-1 cells and the TRAF1 V203A cells, suggesting that NF-κB activation is not the cause of the observed decrease inflammasome activation in TRAF1 V203A cells. Interestingly, there does seem to be a slight decrease in expression of pro-IL-1β in the TRAF1 V203A cells compared to WT THP-1 cells. This decrease in the production of the precursor of mature IL-1β may contribute to the decreased secretion of IL-1β observed. Our lab has also produced preliminary results suggesting that linear ubiquitination of ASC via LUBAC is unaffected in TRAF1 V203A cells, potentially eliminating that interaction as the cause of the observed inhibition of inflammasome activation. However, more research is required to better understand the mechanism in which this TRAF1 V203A

mutation specifically contributed to the lessened inflammasome activation observed in this thesis.

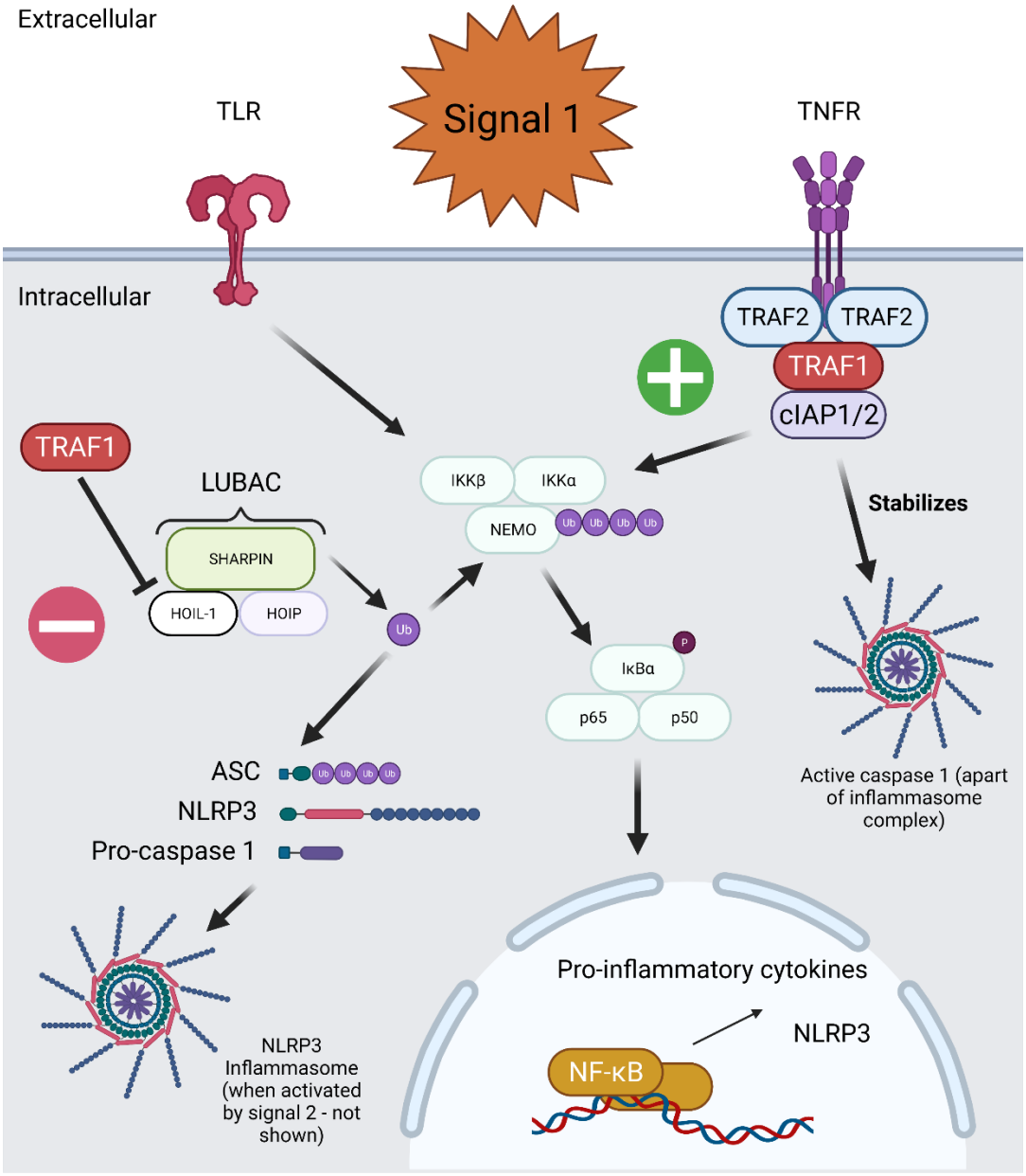

Figure 15. *Multi-facetted role of TRAF1 in NLRP3 inflammasome activation.*

Chapter Six: Future Directions

To continue the progress made in this study, more analysis into role that TRAF1 plays in the in-vivo models of inflammatory disease could unlock more mechanistic insight and opportunity for comparisons between disease progression in humans. To that end, the in-vivo models used in this study could be employed to assess, more specifically, the mechanism in which TRAF1 controls inflammasome activation. This could be done by assessing ubiquitination and oligomerization of ASC in murine bone-marrow derived macrophages and using the disease-models employed in this study to transgenic mice with modified activity of LUBAC and cIAPs, on their own and in conjunction with the TRAF1 KO. Further analysis regarding gene expression of the pro-inflammatory chemokines MCP5 and CxCL10 that were downregulated in crystal-induced arthritis is an intriguing avenue for further exploration. Incidence of autoimmune disease like RA also disproportionately affect females[75]. Assessment of these disease models to specifically assess sex-specific disease progression and its relation to TRAF1 is another important step in determining TRAF1's specific role in inflammatory diseases. These further experiments would serve to further analyze the components of inflammasome activation already identified to be affected by TRAF1 in-vitro such that more physiologically relevant conclusions about the role of TRAF1 in inflammasome activation and its relation to pathogenesis of inflammatory diseases like RA can be determined.

To further assess the specific interaction sites of TRAF1 and their role in inflammation, more analysis on the TRAF1 V203A cells is required. To this end, our lab will continue to examine cIAP2 expression and activity in these cells, including its ability to complete K63-ubiquinitation of caspase-1, which we hypothesize will be downregulated since cIAP2 cannot interact with TRAF1 to maintain its stability. Further analysis of LUBAC's interaction with

NEMO and ASC in the TRAF1 V203A cells will also narrow down then mechanism in which inflammasome activation is inhibited by this mutation. Moreover, we will create the other TRAF1 mutant S283A that maintains interaction with cIAP2 and fails to bind to HOIL-1 subunit of LUBAC. Then, we will conduct experiments to assess how the presence of TRAF1 would affect the inflammatory response through NLRP3 activation and processing of downstream products such as caspase-1 and IL-1β. This would be an additional way to examine the role of TRAF1 on NLRP3 inflammasome activation independent of its role on regulation of NF-κB activation downstream of TNFR.

References

1. Moretti, J. & Blander, J. M. Increasing complexity of NLRP3 inflammasome regulation. *J Leukoc Biol* **109**, 561–571 (2021).

2. Spel, L. & Martinon, F. Inflammasomes contributing to inflammation in arthritis. *Immunol Rev* **294**, 48–62 (2020).

3. Broz, P. & Dixit, V. M. Inflammasomes: mechanism of assembly, regulation and signalling. *Nat Rev Immunol* **16**, 407–420 (2016).

4. Guo, H., Callaway, J. B. & Ting, J. P.-Y. Inflammasomes: mechanism of action, role in disease, and therapeutics. *Nat Med* **21**, 677–687 (2015).

5. Martinon, F. & Tschopp, J. NLRs join TLRs as innate sensors of pathogens. *Trends in Immunology* **26**, 447–454 (2005).

6. Kumar, H., Kawai, T. & Akira, S. Pathogen Recognition by the Innate Immune System. *International Reviews of Immunology* **30**, 16–34 (2011).

7. He, W. *et al.* Gasdermin D is an executor of pyroptosis and required for interleukin-1β secretion. *Cell Res* **25**, 1285–1298 (2015).

8. Santoni, G. *et al.* Danger- and pathogen-associated molecular patterns recognition by pattern-recognition receptors and ion channels of the transient receptor potential family triggers the inflammasome activation in immune cells and sensory neurons. *J Neuroinflammation* **12**, (2015).

9. Sahoo, B. R. Structure of fish Toll-like receptors (TLR) and NOD-like receptors (NLR). *Int J Biol Macromol* **161**, 1602–1617 (2020).

10. Tartey, S. & Takeuchi, O. Pathogen recognition and Toll-like receptor targeted therapeutics in innate immune cells. *International Reviews of Immunology* **36**, 57–73 (2017).

11. Medzhitov, R. & Janeway, C. A. Innate immunity: impact on the adaptive immune response. *Current Opinion in Immunology* **9**, 4–9 (1997).

12. Dolasia, K., Bisht, M. K., Pradhan, G., Udgata, A. & Mukhopadhyay, S. TLRs/NLRs: Shaping the landscape of host immunity. *International Reviews of Immunology* **37**, 3–19 (2018).

13. Takeda, K. Toll-like receptors in innate immunity. *International Immunology* **17**, 1–14 (2004).

14. Akira, S., Uematsu, S. & Takeuchi, O. Pathogen Recognition and Innate Immunity. *Cell* **124**, 783–801 (2006).

15. Delneste, Y., Beauvillain, C. & Jeannin, P. Immunité naturelle: Structure et fonction des *Toll-like receptors*. *Med Sci (Paris)* **23**, 67–74 (2007).

16. Kawai, T. & Kawasaki, T. Toll-like receptor signaling pathways. *Frontiers in Immunology* **5**, 1–8 (2014).

17. Fitzgerald, K. A. & Kagan, J. C. Toll-like Receptors and the Control of Immunity. *Cell* **180**, 1044–1066 (2020).

18. Su, Q. *et al.* Effects of the TLR4/Myd88/NF-κB Signaling Pathway on NLRP3 Inflammasome in Coronary Microembolization-Induced Myocardial Injury. *Cell Physiol Biochem* **47**, 1497–1508 (2018).

19. Verstrepen, L. *et al.* TLR-4, IL-1R and TNF-R signaling to NF-κB: variations on a common theme. *Cell. Mol. Life Sci.* **65**, 2964–2978 (2008).

20. Kelley, N., Jeltema, D., Duan, Y. & He, Y. The NLRP3 Inflammasome: An Overview of Mechanisms of Activation and Regulation. *IJMS* **20**, 3328 (2019).

21. Lamkanfi, M. *et al.* Inflammasome-Dependent Release of the Alarmin HMGB1 in Endotoxemia. *J Immunol* **185**, 4385–4392 (2010).

22. Chen, G., Shaw, M. H., Kim, Y.-G. & Nuñez, G. NOD-Like Receptors: Role in Innate Immunity and Inflammatory Disease. *Annu. Rev. Pathol. Mech. Dis.* **4**, 365–398 (2009).

23. Corridoni, D., Arseneau, K. O., Cifone, M. G. & Cominelli, F. The Dual Role of Nod-Like Receptors in Mucosal Innate Immunity and Chronic Intestinal Inflammation. *Front. Immunol.* **5**, (2014).

24. Schroder, K. & Tschopp, J. The Inflammasomes. *Cell* **140**, 821–832 (2010).

25. Lamkanfi, M. & Dixit, V. M. Mechanisms and Functions of Inflammasomes. *Cell* **157**, 1013–1022 (2014).

26. Platnich, J. M. & Muruve, D. A. NOD-like receptors and inflammasomes: A review of their canonical and non-canonical signaling pathways. *Archives of Biochemistry and Biophysics* **670**, 4–14 (2019).

27. de Zoete, M. R., Palm, N. W., Zhu, S. & Flavell, R. A. Inflammasomes. *Cold Spring Harb Perspect Biol* **6**, (2014).

28. Huang, M. T.-H. *et al.* Critical Role of Apoptotic Speck Protein Containing a Caspase Recruitment Domain (ASC) and NLRP3 in Causing Necrosis and ASC Speck Formation Induced by *Porphyromonas gingivalis* in Human Cells. *J Immunol* **182**, 2395–2404 (2009).

29. Dick, M. S., Sborgi, L., Rühl, S., Hiller, S. & Broz, P. ASC filament formation serves as a signal amplification mechanism for inflammasomes. *Nat Commun* **7**, 11929 (2016).

30. Kufer, T. A. & Sansonetti, P. J. NLR functions beyond pathogen recognition. *Nat Immunol* **12**, 121–128 (2011).

31. Lamkanfi, M. & Dixit, V. M. Inflammasomes and Their Roles in Health and Disease. *Annu. Rev. Cell Dev. Biol.* **28**, 137–161 (2012).

32. Stehlik, C. *et al.* The PAAD/PYRIN-only protein POP1/ASC2 is a modulator of ASC-mediated nuclear-factor-κB and pro-caspase-1 regulation. 13 (2003).

33. Kaneko, N., Kurata, M., Yamamoto, T., Morikawa, S. & Masumoto, J. The role of interleukin-1 in general pathology. *Inflamm Regener* **39**, 12 (2019).

34. McAllister, M. J., Chemaly, M., Eakin, A. J., Gibson, D. S. & McGilligan, V. E. NLRP3 as a potentially novel biomarker for the management of osteoarthritis. *Osteoarthritis and Cartilage* **26**, 612–619 (2018).

35. Fusco, R., Siracusa, R., Genovese, T., Cuzzocrea, S. & Di Paola, R. Focus on the Role of NLRP3 Inflammasome in Diseases. *Int J Mol Sci* **21**, (2020).

36. Edilova, M. I., Akram, A. & Abdul-Sater, A. A. Innate immunity drives pathogenesis of rheumatoid arthritis. *Biomedical Journal* S2319417020300986 (2020) doi:10.1016/j.bj.2020.06.010.

37. Dinarello, C. A. Interleukin-1 in the pathogenesis and treatment of inflammatory diseases. *Blood* **117**, 3720–3732 (2011).

38. Elinav, E., Strowig, T., Henao-Mejia, J. & Flavell, R. A. Regulation of the Antimicrobial Response by NLR Proteins. *Immunity* **34**, 665–679 (2011).

39. Gross, O., Thomas, C. J., Guarda, G. & Tschopp, J. The inflammasome: an integrated view. *Immunological Reviews* **243**, 136–151 (2011).

40. Davis, B. K., Wen, H. & Ting, J. P.-Y. The Inflammasome NLRs in Immunity, Inflammation, and Associated Diseases. *Annu. Rev. Immunol.* **29**, 707–735 (2011).

41. Groslambert, M. & Py, B. F. Spotlight on the NLRP3 inflammasome pathway. *J Inflamm Res* **11**, 359–374 (2018).

42. Muñoz-Planillo, R. *et al.* K+ efflux is the Common Trigger of NLRP3 inflammasome Activation by Bacterial Toxins and Particulate Matter. *Immunity* **38**, 1142–1153 (2013).

43. Di, A. *et al.* The TWIK2 Potassium Efflux Channel in Macrophages Mediates NLRP3 Inflammasome-Induced Inflammation. *Immunity* **49**, 56-65.e4 (2018).

44. McKee, C. M. & Coll, R. C. NLRP3 inflammasome priming: A riddle wrapped in a mystery inside an enigma. *Journal of Leukocyte Biology* **108**, 937–952 (2020).

45. Murakami, T. *et al.* Critical role for calcium mobilization in activation of the NLRP3 inflammasome. *Proc Natl Acad Sci U S A* **109**, 11282–11287 (2012).

46. Wang, S. *et al.* S100A8/A9 in Inflammation. *Front. Immunol.* **9**, 1298 (2018).

47. Han, J. *et al.* Preventive effect of dioscin against monosodium urate-mediated gouty arthritis through inhibiting inflammasome NLRP3 and TLR4/NF-κB signaling pathway activation: an in vivo and in vitro study. *J Nat Med* **75**, 37–47 (2021).

48. Martinon, F., Pétrilli, V., Mayor, A., Tardivel, A. & Tschopp, J. Gout-associated uric acid crystals activate the NALP3 inflammasome. *Nature* **440**, 237–241 (2006).

49. Goldberg, E. L. *et al.* β-hydroxybutyrate deactivates neutrophil NLRP3 inflammasome to relieve gout flares. *Cell Rep* **18**, 2077–2087 (2017).

50. Bai, H. Cathepsin B Regulates the Activation of NLRP3 Inflammasome by Calcium Signaling. 14 (2018).

51. Amaral, E. P. *et al.* Lysosomal Cathepsin Release Is Required for NLRP3-Inflammasome Activation by Mycobacterium tuberculosis in Infected Macrophages. *Front. Immunol.* **9**, 1427 (2018).

52. Välimäki, E., Miettinen, J. J., Lietzén, N., Matikainen, S. & Nyman, T. A. Monosodium Urate Activates Src/Pyk2/PI3 Kinase and Cathepsin Dependent Unconventional Protein Secretion From Human Primary Macrophages. *Mol Cell Proteomics* **12**, 749–763 (2013).

53. Spalinger, M. & Scharl, M. Mono Sodium Urate Crystal-induced Peritonitis for in vivo Assessment of Inflammasome Activation. *BIO-PROTOCOL* **8**, (2018).

54. Baker, P. J. *et al.* Posttranslational Modification as a Critical Determinant of Cytoplasmic Innate Immune Recognition. *Physiological Reviews* **97**, 1165–1209 (2017).

55. Rodgers, M. A. *et al.* The linear ubiquitin assembly complex (LUBAC) is essential for NLRP3 inflammasome activation. *Journal of Experimental Medicine* **211**, 1333–1347 (2014).

56. Bednash, J. S. & Mallampalli, R. K. Regulation of inflammasomes by ubiquitination. *Cell Mol Immunol* **13**, 722–728 (2016).

57. Abdul-Sater, A. A. *et al.* The signaling adaptor TRAF1 negatively regulates Toll-like receptor signaling and this underlies its role in rheumatic disease. *Nat Immunol* **18**, 26–35 (2017).

58. Shen, H.-H. *et al.* NLRP3: A promising therapeutic target for autoimmune diseases. *Autoimmunity Reviews* **17**, 694–702 (2018).

59. Kolly, L. *et al.* Expression and function of the NALP3 inflammasome in rheumatoid synovium. *Immunology* **129**, 178–185 (2010).

60. Shin, J. I. *et al.* Inflammasomes and autoimmune and rheumatic diseases: A comprehensive review. *Journal of Autoimmunity* **103**, 102299 (2019).

61. Guo, C. *et al.* NLRP3 inflammasome activation contributes to the pathogenesis of rheumatoid arthritis. *Clin Exp Immunol* **194**, 231–243 (2018).

62. Choulaki, C. *et al.* Enhanced activity of NLRP3 inflammasome in peripheral blood cells of patients with active rheumatoid arthritis. *Arthritis Res Ther* **17**, 257 (2015).

63. Zhong, Z., Sanchez-Lopez, E. & Karin, M. Autophagy, NLRP3 inflammasome and auto-inflammatory/immune diseases. 5.

64. Xie, P. TRAF molecules in cell signaling and in human diseases. 31 (2013).

65. Edilova, M. I., Abdul-Sater, A. A. & Watts, T. H. TRAF1 Signaling in Human Health and Disease. *Front. Immunol.* **9**, 2969 (2018).

66. Zapata, J. M. & Reed, J. C. TRAF1: Lord Without a RING. *Science's STKE* **27**, 1–5 (2002).

67. Tsitsikov, E. N. *et al.* TRAF1 Is a Negative Regulator of TNF Signaling: Enhanced TNF Signaling in TRAF1-Deficient Mice. 11.

68. Griewahn, L., Köser, A. & Maurer, U. Keeping Cell Death in Check: Ubiquitylation-Dependent Control of TNFR1 and TLR Signaling. *Front. Cell Dev. Biol.* **7**, 117 (2019).

69. Tokunaga, F. *et al.* Involvement of linear polyubiquitylation of NEMO in NF-κB activation. *Nat Cell Biol* **11**, 123–132 (2009).

70. Gurung, P., Lamkanfi, M. & Kanneganti, T.-D. Cutting Edge: SHARPIN Is Required for Optimal NLRP3 Inflammasome Activation. *J.I.* **194**, 2064–2067 (2015).

71. Szekanecz, Z., Szamosi, S., Kovács, G. E., Kocsis, E. & Benkő, S. The NLRP3 inflammasome - interleukin 1 pathway as a therapeutic target in gout. *Archives of Biochemistry and Biophysics* **670**, 82–93 (2019).

72. Szekanecz, Z., Vegvari, A., Szabo, Z. & Koch, A. E. Chemokines and chemokine receptors in arthritis. *Front Biosci (Schol Ed)* **2**, 153–167 (2010).

73. Ragab, G., Elshahaly, M. & Bardin, T. Gout: An old disease in new perspective – A review. *J Adv Res* **8**, 495–511 (2017).

74. Labbé, K., McIntire, C. R., Doiron, K., Leblanc, P. M. & Saleh, M. Cellular Inhibitors of Apoptosis Proteins cIAP1 and cIAP2 Are Required for Efficient Caspase-1 Activation by the Inflammasome. *Immunity* **35**, 897–907 (2011).

75. Whitacre, C. C. Sex differences in autoimmune disease. *Nature Immunology* **2**, 777–780 (2001).